Numerical analysis of superconducting phases in the extended Hubbard model with non-local pairing

University of Pisa, a.y. 2025-2026

Alessandro Gori*

Thesis for the Master's degree in Physics

Abstract

[To be continued...]

Contents

Draft: December 27, 2025

*a.gori23@studenti.unipi.it / nepero27178@github.com

List of symbols and abbreviations

AF	Anti-Ferromagnetic
BCS	Bardeen-Cooper-Schrieffer (theory)
DoF	Degree of Freedom
HF	Hartree-Fock
HFPs	Hartree-Fock parameters
LRT	Linear Response Theory
MFT	Mean-Field Theory
SC	Superconductor
SSB	Spontaneous Symmetry Breaking
T_c	Critical temperature

Part I

Mean-Field-Theory analysis

Chapter 1

Anti-Ferromagnetic instability

In this chapter, the effect of the non-local interaction on the antiferromagnetic phase is discussed. The MFT derivation for the Hubbard Model is discussed in App. A.

1.1 Symmetry considerations for the AF phase

[To be continued...]

1.2 Antiferromagnetism in the conventional Hubbard model

The Anti-Ferromagnetic phase, specified by the Ansatz (A.2) (which is explicitly breaking translational invariance in each spin sector, while preserving $\mathrm{U}^z(1)$ and $\mathrm{U}^c(1)$ symmetries) reduces the hamiltonian to the form of Eq. (A.3)

$$\hat{H}_t + \hat{H}_U \overset{\text{MFT}}{\simeq} -t \sum_{\langle \mathbf{r}\mathbf{r}' \rangle} \sum_{\sigma} \hat{c}^\dagger_{\mathbf{r}\sigma} \hat{c}_{\mathbf{r}'\sigma} + nU \sum_{\mathbf{r}} [\hat{n}_{\mathbf{r}\uparrow} + \hat{n}_{\mathbf{r}\downarrow}] - mU \sum_{\mathbf{r}} (-1)^{x+y} [\hat{n}_{\mathbf{r}\uparrow} - \hat{n}_{\mathbf{r}\downarrow}]$$

In reciprocal space, the hamiltonian decomposes as in Eq. (A.5),

$$\hat{H}_t + \hat{H}_U \overset{\text{MFT}}{\simeq} \sum_{\mathbf{k}\in \text{MBZ}} \sum_{\sigma} \hat{\Psi}^\dagger_{\mathbf{k}\sigma} h_{\mathbf{k}\sigma} \hat{\Psi}_{\mathbf{k}\sigma} \quad \text{being} \quad h_{\mathbf{k}\sigma} \equiv \begin{bmatrix} \epsilon_{\mathbf{k}} & -\Delta_\sigma \\ -\Delta_\sigma & -\epsilon_{\mathbf{k}} \end{bmatrix}$$

and $\Delta_\uparrow = mU$, $\Delta_\downarrow = -mU$. Nambu spinorial formulation is used,

$$\hat{\Psi}_{\mathbf{k}\sigma} \equiv \begin{bmatrix} \hat{c}_{\mathbf{k}\sigma} \\ \hat{c}_{\mathbf{k}+\boldsymbol{\pi}\sigma} \end{bmatrix}$$

and the free electrons energy is simply the tight binding energy

$$\epsilon_{\mathbf{k}} = -2t \left[\cos(k_x) + \cos(k_y)\right]$$

which is spin-invariant. The MFT description of the model reduces to a gas of free "γ-fermions", described by the Nambu spinor of Eq. (A.10),

$$\hat{\Gamma}_{\mathbf{k}\sigma} = W_{\mathbf{k}\sigma} \hat{\Psi}_{\mathbf{k}\sigma} = \begin{bmatrix} \hat{\gamma}^{(-)}_{\mathbf{k}\sigma} \\ \hat{\gamma}^{(+)}_{\mathbf{k}\sigma} \end{bmatrix}$$

where

$$W_{\mathbf{k}\sigma} = \begin{bmatrix} -\sin\theta_{\mathbf{k}\sigma} & -\cos\theta_{\mathbf{k}\sigma} \\ \cos\theta_{\mathbf{k}\sigma} & -\sin\theta_{\mathbf{k}\sigma} \end{bmatrix} \quad \text{and} \quad \sin 2\theta_{\mathbf{k}\sigma} \equiv \frac{\Delta_\sigma}{E_{\mathbf{k}}}$$

These fermions populate the two bands $\pm E_{\mathbf{k}} = \sqrt{\epsilon^2_{\mathbf{k}} + \Delta^2}$. The entire system is mapped onto an ensemble of pseudo-spins, each subject to a pseudo-field, as in Fig. 1.1. To diagonalize the system

essentially means to align each pseudo-spin with the z axis. Within on the notation of Fig. A.3, the following expectations values hold:

$$\langle\hat{\Psi}^\dagger_{\mathbf{k}\sigma}\tau^x\hat{\Psi}_{\mathbf{k}\sigma}\rangle = \sin(2\theta_{\mathbf{k}})\langle\hat{\Gamma}^\dagger_{\mathbf{k}\sigma}\tau^z\hat{\Gamma}_{\mathbf{k}\sigma}\rangle \tag{1.1}$$

$$\langle\hat{\Psi}^\dagger_{\mathbf{k}\sigma}\tau^y\hat{\Psi}_{\mathbf{k}\sigma}\rangle = 0 \tag{1.2}$$

$$\langle\hat{\Psi}^\dagger_{\mathbf{k}\sigma}\tau^z\hat{\Psi}_{\mathbf{k}\sigma}\rangle = -\cos(2\theta_{\mathbf{k}})\langle\hat{\Gamma}^\dagger_{\mathbf{k}\sigma}\tau^z\hat{\Gamma}_{\mathbf{k}\sigma}\rangle \tag{1.3}$$

and since the γ-fermions are free and in the rotated frame the pseudo-field points "up",

$$\langle\hat{\Gamma}^\dagger_{\mathbf{k}\sigma}\tau^z\hat{\Gamma}_{\mathbf{k}\sigma}\rangle = \frac{1}{2}\left[f\left(-E_{\mathbf{k}};\beta,\tilde{\mu}\right) - f\left(E_{\mathbf{k}};\beta,\tilde{\mu}\right)\right]$$

1.3 EHM model and antiferromagnetic ordering

Consider now the non-local interaction $\hat{H}_V$: since only translational invariance is broken in the AF phase, the only relevant contributions coming from Wick's decomposition are Hartree terms and the same-spin Fock term. The net effect obtained by including this interaction, as I will explain, is a renormalization of the various quantities,

$$\epsilon_{\mathbf{k}} \to \tilde{\epsilon}_{\mathbf{k}\sigma} \qquad E_{\mathbf{k}} \to \tilde{E}_{\mathbf{k}\sigma} \qquad \Delta_\sigma \to \tilde{\Delta}_{\mathbf{k}\sigma} \qquad \theta_{\mathbf{k}\sigma} \to \tilde{\theta}_{\mathbf{k}\sigma} \qquad W_{\mathbf{k}\sigma} \to \tilde{W}_{\mathbf{k}\sigma}$$

The band energies renormalization is simply

$$\tilde{E}_{\mathbf{k}\sigma} \equiv \sqrt{\tilde{\epsilon}^2_{\mathbf{k}\sigma} + |\tilde{\Delta}_{\mathbf{k}\sigma}|^2}$$

and the following relations hold:

$$\langle\hat{\Psi}^\dagger_{\mathbf{k}\sigma}\tau^x\hat{\Psi}_{\mathbf{k}\sigma}\rangle = \sin(2\tilde{\theta}_{\mathbf{k}})\sin(2\tilde{\zeta}_{\mathbf{k}})\langle\hat{\Gamma}^\dagger_{\mathbf{k}\sigma}\tau^z\hat{\Gamma}_{\mathbf{k}\sigma}\rangle \tag{1.4}$$

$$\langle\hat{\Psi}^\dagger_{\mathbf{k}\sigma}\tau^y\hat{\Psi}_{\mathbf{k}\sigma}\rangle = \sin(2\tilde{\theta}_{\mathbf{k}})\cos(2\tilde{\zeta}_{\mathbf{k}})\langle\hat{\Gamma}^\dagger_{\mathbf{k}\sigma}\tau^z\hat{\Gamma}_{\mathbf{k}\sigma}\rangle \tag{1.5}$$

$$\langle\hat{\Psi}^\dagger_{\mathbf{k}\sigma}\tau^z\hat{\Psi}_{\mathbf{k}\sigma}\rangle = -\cos(2\tilde{\theta}_{\mathbf{k}})\langle\hat{\Gamma}^\dagger_{\mathbf{k}\sigma}\tau^z\hat{\Gamma}_{\mathbf{k}\sigma}\rangle \tag{1.6}$$

with:

$$\sin(2\tilde{\xi}_{\mathbf{k}}) = \frac{\mathrm{Re}\{\tilde{\Delta}_{\mathbf{k}}\}}{|\tilde{\Delta}_{\mathbf{k}}|} \qquad \cos(2\tilde{\xi}_{\mathbf{k}}) = \frac{\mathrm{Im}\{\tilde{\Delta}_{\mathbf{k}}\}}{|\tilde{\Delta}_{\mathbf{k}}|} \qquad \sin(2\tilde{\theta}_{\mathbf{k}}) = \frac{|\tilde{\Delta}_{\mathbf{k}}|}{\tilde{E}_{\mathbf{k}}} \qquad \cos(2\tilde{\theta}_{\mathbf{k}}) = \frac{\tilde{\epsilon}_{\mathbf{k}}}{\tilde{E}_{\mathbf{k}}} \tag{1.7}$$

The physical behavior is the same as for the pure Hubbard model. In next sections the different contributions to renormalization are treated.

1.3.1 Hartree renormalization of chemical potential and gap

The same-spin and opposite-spin non-local Hartree terms are

$$\underbrace{-V\sum_{\langle ij\rangle}\sum_{\sigma}\left[\langle\hat{n}_{i\sigma}\rangle\hat{n}_{j\sigma} + \hat{n}_{i\sigma}\langle\hat{n}_{j\sigma}\rangle\right]}_{\text{s.s.}} \underbrace{-V\sum_{\langle ij\rangle}\sum_{\sigma}\left[\langle\hat{n}_{i\sigma}\rangle\hat{n}_{j\bar{\sigma}} + \hat{n}_{i\sigma}\langle\hat{n}_{j\bar{\sigma}}\rangle\right]}_{\text{o.s.}}$$

Let $i \to \mathbf{r} = (x, y)$ and $j \to \mathbf{r}' = (x', y')$. Then, using the Ansatz of Eq. (A.2), summarized as

$$\langle\hat{n}_{\mathbf{r}\sigma}\rangle = n - (-1)^{x+y+\delta_{\sigma=\uparrow}}m$$

we get

$$\overbrace{\begin{aligned}&-nV\sum_{\langle\mathbf{r}\mathbf{r}'\rangle}\sum_{\sigma}\left[\hat{n}_{\mathbf{r}'\sigma} + \hat{n}_{\mathbf{r}\sigma}\right] + mV\sum_{\langle\mathbf{r}\mathbf{r}'\rangle}\sum_{\sigma}(-1)^{\delta_{\sigma=\uparrow}}\left[(-1)^{x'+y'}\hat{n}_{\mathbf{r}'\sigma} + (-1)^{x+y}\hat{n}_{\mathbf{r}\sigma}\right]\\ &\underbrace{-nV\sum_{\langle\mathbf{r}\mathbf{r}'\rangle}\sum_{\sigma}\left[\hat{n}_{\mathbf{r}'\bar{\sigma}} + \hat{n}_{\mathbf{r}\sigma}\right] + mV\sum_{\langle\mathbf{r}\mathbf{r}'\rangle}\sum_{\sigma}\left[(-1)^{x'+y'+\delta_{\bar{\sigma}=\uparrow}}\hat{n}_{\mathbf{r}'\bar{\sigma}} + (-1)^{x+y+\delta_{\sigma=\uparrow}}\hat{n}_{\mathbf{r}\sigma}\right]}_{\text{o.s.}}\end{aligned}}^{\text{s.s.}}$$

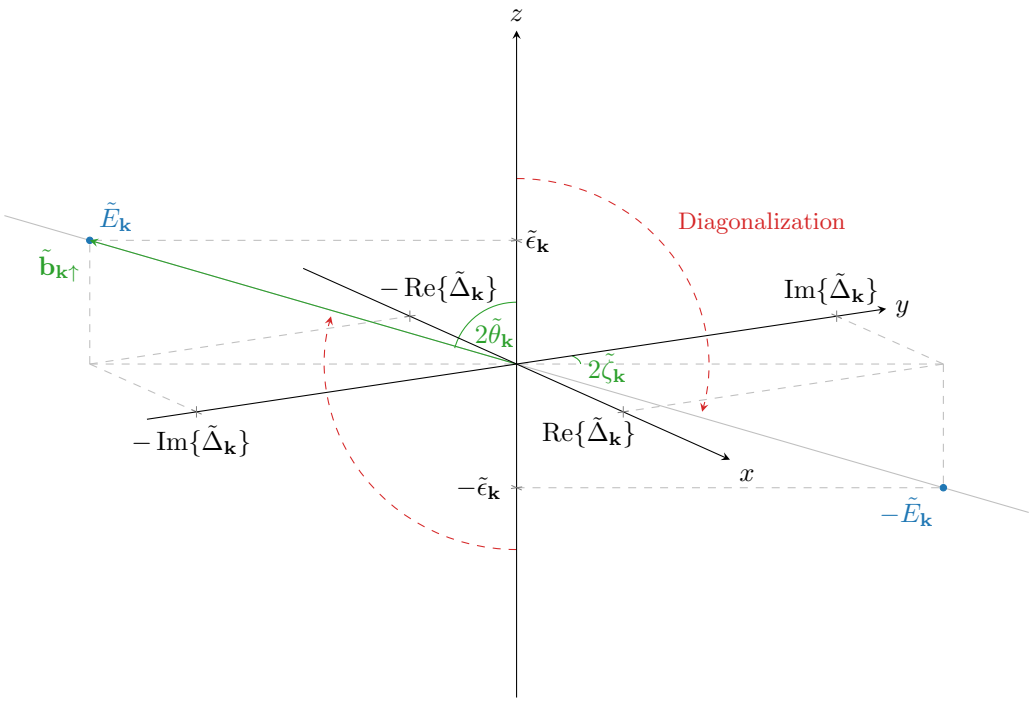

Figure 1.1 | Sketch of the diagonalization of the pseudo-spin problem. The dashed line represents the diagonalization given by the z-axis alignment with the field direction. In the top-right side of the picture are listed the expectation values of the original Nambu spinor.

For a square lattice, if $\mathbf{r} = (x, y)$ and $\mathbf{r}' = (x', y')$ are NNs evidently

$$(-1)^{x'+y'} = (-1)^{x+y+1}$$

Moreover,

$$(-1)^{\delta_{\bar{\sigma}=\uparrow}} = (-1)^{\delta_{\sigma=\uparrow}+1}$$

We obtain

$$\overbrace{-nV \sum_{\langle \mathbf{r}\mathbf{r}' \rangle} \sum_{\sigma} [\hat{n}_{\mathbf{r}\sigma} + \hat{n}_{\mathbf{r}'\sigma}]}^{\text{s.s. (density)}} + \overbrace{mV \sum_{\langle \mathbf{r}\mathbf{r}' \rangle} \sum_{\sigma} (-1)^{x+y+\delta_{\sigma=\uparrow}} [\hat{n}_{\mathbf{r}\sigma} - \hat{n}_{\mathbf{r}'\sigma}]}^{\text{s.s. (magnetization)}}$$
$$\underbrace{-nV \sum_{\langle \mathbf{r}\mathbf{r}' \rangle} \sum_{\sigma} [\hat{n}_{\mathbf{r}\sigma} + \hat{n}_{\mathbf{r}'\bar{\sigma}}]}_{\text{o.s. (density)}} + \underbrace{mV \sum_{\langle \mathbf{r}\mathbf{r}' \rangle} \sum_{\sigma} (-1)^{x+y+\delta_{\sigma=\uparrow}} [\hat{n}_{\mathbf{r}\sigma} + \hat{n}_{\mathbf{r}'\bar{\sigma}}]}_{\text{o.s. (magnetization)}} \tag{1.8}$$

In the above expressions the various contribution have been separated in "density" contributions and "magnetization" contributions. Let me deal with these separately.

Density terms. Consider the *s.s.* and *o.s.* (density) terms of Expr. (1.8). Since

$$\sum_{\langle \mathbf{r}\mathbf{r}' \rangle} \sum_{\sigma} [\hat{n}_{\mathbf{r}\sigma} + \hat{n}_{\mathbf{r}'\sigma}] = \sum_{\langle \mathbf{r}\mathbf{r}' \rangle} \sum_{\sigma} [\hat{n}_{\mathbf{r}\sigma} + \hat{n}_{\mathbf{r}'\bar{\sigma}}] = z\hat{N}$$

with $z = 4$ the lattice coordination factor, indicating the number of NNs per site, then the first and third terms of Expr. (1.8) contribute to a pure chemical potential shift. The renormalized chemical potential is:

$$\tilde{\mu} \equiv \mu + 2znV \tag{1.9}$$

Magnetization terms. The s.s. and o.s. (magnetization) terms of Expr. (1.8) are to be reduced to a renormalization of the gap function. Explicitly,

$$mV\sum_{\langle \mathbf{r}\mathbf{r}'\rangle}\sum_{\sigma}(-1)^{x+y+\delta_{\sigma=\uparrow}}\left[\hat{n}_{\mathbf{r}\sigma}-\hat{n}_{\mathbf{r}'\sigma}\right]+mV\sum_{\langle \mathbf{r}\mathbf{r}'\rangle}\sum_{\sigma}(-1)^{x+y+\delta_{\sigma=\uparrow}}\left[\hat{n}_{\mathbf{r}\sigma}+\hat{n}_{\mathbf{r}'\bar{\sigma}}\right]$$
$$=-2zmV\sum_{\mathbf{r}}(-1)^{x+y}\left[\hat{n}_{\mathbf{r}\uparrow}-\hat{n}_{\mathbf{r}\downarrow}\right] \quad (1.10)$$

Consider now the last term of the pure Hubbard model under MFT approximations of Eq. (A.3),

$$-mU\sum_{\mathbf{r}}(-1)^{x+y}\left[\hat{n}_{\mathbf{r}\uparrow}-\hat{n}_{\mathbf{r}\downarrow}\right] \quad \text{(Local gap)}$$

Expr. (1.10) is formally identical, thus we obtain a contribution to the renormalization of the AF gap,

$$\Delta\to\Delta+2zmV+(\text{s.s. contribution}) \quad (1.11)$$

This, together with Eq. (1.9), concludes the non-local Hartree reparametrization of the hamiltonian. Next section is devoted to analyzing the effect of the Fock term.

1.3.2 Fock renormalization of the hopping amplitude

From Wick's decomposition of $\hat{H}_V$, the only allowed Fock term comes from the same-spin part due to SU(2) symmetry selection rules. Said hamiltonian term is

$$V\sum_{\langle ij\rangle}\sum_{\sigma}\left[\langle\hat{c}^{\dagger}_{i\sigma}\hat{c}_{j\sigma}\rangle\hat{c}^{\dagger}_{j\sigma}\hat{c}_{i\sigma}+h.c.\right] \quad (1.12)$$

(note the + sign in front of it). A bond-wise hopping amplitude can be defined,

$$\tilde{t}_{ij\sigma}\equiv t-V\langle\hat{c}^{\dagger}_{j\sigma}\hat{c}_{i\sigma}\rangle$$

In the AF phase, given some site i and a spin σ, evidently $\tilde{t}_{ij\sigma}$ must be identical for any NN site j. Over the planar square lattice, this implies that the quantity $\langle\hat{c}^{\dagger}_{j\sigma}\hat{c}_{i\sigma}\rangle$ exhibits s^*-wave symmetry (also referred to as "Extended s-wave symmetry"). Later in the text, different symmetry structures will be discussed thoroughly. For now, the s^*-wave symmetry is the one given in Tab. **??** and depicted in Fig. **??**. These considerations will become useful later. The effective diffusive hamiltonian is given by

$$\hat{H}_{\tilde{t}}=\hat{H}_t+V\sum_{\langle ij\rangle}\sum_{\sigma}\left[\langle\hat{c}^{\dagger}_{i\sigma}\hat{c}_{j\sigma}\rangle\hat{c}^{\dagger}_{j\sigma}\hat{c}_{i\sigma}+h.c.\right]$$
$$=-\sum_{\langle ij\rangle}\sum_{\sigma}\left[\tilde{t}_{ij\sigma}\hat{c}^{\dagger}_{i\sigma}\hat{c}_{j\sigma}+h.c.\right]$$

As will become clear in next section, not only the diffusive part of the hamiltonian actually is affected by the Fock renormalization; also the gap terms are effectively renormalized.

In reciprocal space, the effective hopping must be transformed as well. Consider the Fourier Transform given in Eq. (**??**), applied to Eq. (1.12),

$$V\sum_{\langle ij\rangle}\sum_{\sigma}\left[\langle\hat{c}^{\dagger}_{i\sigma}\hat{c}_{j\sigma}\rangle\hat{c}^{\dagger}_{j\sigma}\hat{c}_{i\sigma}+h.c.\right]$$
$$=\frac{2V}{L_xL_y}\sum_{\mathbf{K},\mathbf{k},\mathbf{k}'}\sum_{\sigma}\left[\cos(\delta k_x)+\cos(\delta k_y)\right]\langle\hat{c}^{\dagger}_{\mathbf{K}+\mathbf{k}\sigma}\hat{c}_{\mathbf{K}-\mathbf{k}'\sigma}\rangle\hat{c}^{\dagger}_{\mathbf{K}-\mathbf{k}\sigma}\hat{c}_{\mathbf{K}+\mathbf{k}'\sigma} \quad (1.13)$$

where the 2 prefactor comes from recognizing that the $h.c.$ generates an identical contribution to the full sum. In order to proceed, it is now necessary to understand how the AF phase is realized in reciprocal space. As is exposed in App. A, to impose an AF Ansatz of the form

$$\langle\hat{n}_{\mathbf{r}\sigma}\rangle=n-(-1)^{x+y+\delta_{\sigma=\uparrow}}m$$

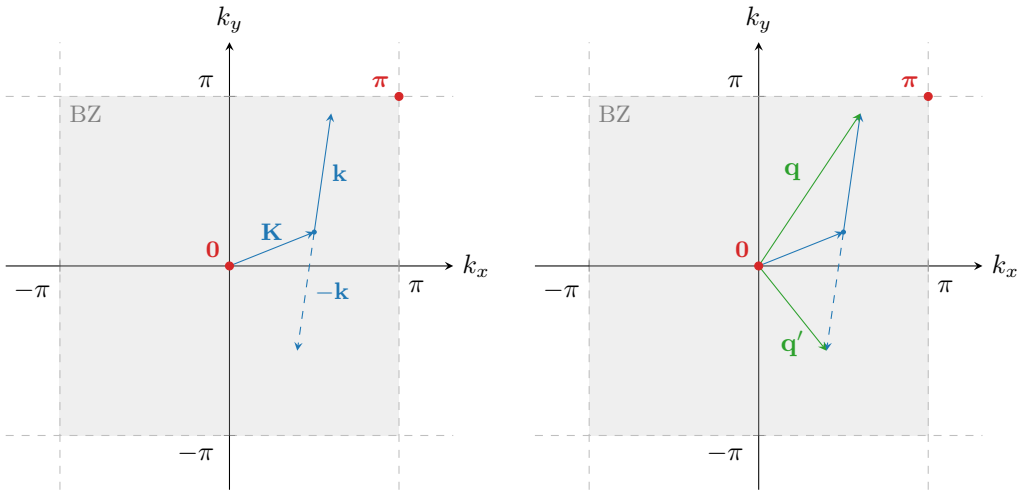

a | Generic vectors. b | Change of variables.

Figure 1.2 | Representation of the vectors involved in the diagonal terms of Eq. (1.14). In Fig. 1.2a generic vectors are considered, cycling over all values of $\mathbf{K}, \mathbf{k} \in \mathrm{BZ}$. In Fig. 1.2b is depicted the variables change to the new vectors $\mathbf{q}, \mathbf{q}'$.

leads to an AF ground-state of free fermions at temperature β described by the Nambu spinor of Eq. (A.10). All parameters are renormalized, thus we must account for renormalized band energies $\pm\tilde{E}_{\mathbf{k}\sigma}$ as well. The ground-state is realized by simply populating the two bands $\pm\tilde{E}_{\mathbf{k}\sigma}$ as

$$\bigotimes_{\mathbf{k}\in\mathrm{MBZ}} \bigotimes_{\sigma} \left[\left(\hat{\gamma}^{(-)}_{\mathbf{k}\sigma}\right)^{\dagger} f(-\tilde{E}_{\mathbf{k}};\beta,\mu) + \left(\hat{\gamma}^{(+)}_{\mathbf{k}\sigma}\right)^{\dagger} f(\tilde{E}_{\mathbf{k}};\beta,\mu) \right] |\Omega\rangle$$

The $\hat{\gamma}$ operators are normalized superpositions of two $\hat{c}$ operators at points in reciprocal space separated by a $\boldsymbol{\pi}$ shift. It follows that the above state is ultimately a superposition of many-body pure states, each of which has either the $\mathbf{k}\sigma$ state occupied *or* the $\mathbf{k}+\boldsymbol{\pi}\sigma$ state for each $\mathbf{k} \in \mathrm{MBZ}$, $\sigma \in \{\uparrow,\downarrow\}$. It follows that, when computing generically $\langle \hat{c}^{\dagger}_{\mathbf{k}_1\sigma}\hat{c}_{\mathbf{k}_2\sigma}\rangle$, such expectation value can be non-zero if and only if $\mathbf{k}_1 = \mathbf{k}_2 + n\boldsymbol{\pi}$, being $n \in \mathbb{Z}$. Going back to Eq. (1.13), this implies only two contributions are non-zero:

$$\mathbf{k} = -\mathbf{k}' \quad \text{or} \quad \mathbf{k}+\boldsymbol{\pi} = -\mathbf{k}'$$

Then Eq. (1.13) is reduced to:

$$\frac{2V}{L_xL_y}\sum_{\mathbf{K},\mathbf{k}}\sum_{\sigma}\left[\cos(2k_x)+\cos(2k_y)\right] \left[\underbrace{\langle \hat{c}^{\dagger}_{\mathbf{K}+\mathbf{k}\sigma}\hat{c}_{\mathbf{K}+\mathbf{k}\sigma}\rangle \hat{c}^{\dagger}_{\mathbf{K}-\mathbf{k}\sigma}\hat{c}_{\mathbf{K}-\mathbf{k}\sigma}}_{\text{Diagonal terms}} - \underbrace{\langle \hat{c}^{\dagger}_{\mathbf{K}+\mathbf{k}\sigma}\hat{c}_{\mathbf{K}+\mathbf{k}+\boldsymbol{\pi}\sigma}\rangle \hat{c}^{\dagger}_{\mathbf{K}-\mathbf{k}\sigma}\hat{c}_{\mathbf{K}-\mathbf{k}-\boldsymbol{\pi}\sigma}}_{\text{Off-diagonal terms}} \right] \tag{1.14}$$

Now, the above equation presents *diagonal* and *off-diagonal* terms. Let me discuss them separately.

Diagonal terms. The diagonal terms of Eq. (1.14) are simple density interactions with the mean density field. Consider Fig. 1.2a: density at vector $\mathbf{q} \equiv \mathbf{K}+\mathbf{k}$ interacts with the mean density at vector $\mathbf{q}' \equiv \mathbf{K}-\mathbf{k}$. These variables are depicted in Fig. 1.2b. Apply the variable change in the diagonal part of Eq. (1.14),

$$\frac{2V}{L_xL_y}\sum_{\mathbf{q},\mathbf{q}'}\sum_{\sigma}\left[\cos(2k_x)+\cos(2k_y)\right]\langle \hat{c}^{\dagger}_{\mathbf{K}+\mathbf{k}\sigma}\hat{c}_{\mathbf{K}+\mathbf{k}\sigma}\rangle \hat{c}^{\dagger}_{\mathbf{K}-\mathbf{k}\sigma}\hat{c}_{\mathbf{K}-\mathbf{k}\sigma}$$
$$= \frac{2V}{L_xL_y}\sum_{\mathbf{q},\mathbf{q}'}\sum_{\sigma}\left[\cos(\delta q_x)+\cos(\delta q_y)\right]\langle \hat{c}^{\dagger}_{\mathbf{q}\sigma}\hat{c}_{\mathbf{q}\sigma}\rangle \hat{c}^{\dagger}_{\mathbf{q}'\sigma}\hat{c}_{\mathbf{q}'\sigma} \tag{1.15}$$

being for $\ell = x, y$

$$\begin{aligned}\delta q_\ell &\equiv q_\ell - q'_\ell \\ &= (K_\ell + k_\ell) - (K_\ell - k_\ell) \\ &= 2k_\ell\end{aligned}$$

The form factor $\cos(\delta q_x) + \cos(\delta q_y)$ decomposes in waves as in Eq. (**??**). In the AF phase, $\langle \hat{c}^\dagger_{\mathbf{q}\sigma} \hat{c}_{\mathbf{q}\sigma} \rangle$ must be s^*-wave symmetric, as anticipated in the starting discussion of Sec. 1.3.2. This is due to the fact that of the four symmetries listed above, only the first one exhibits both x, y reflections symmetry and $\pi/2$ rotational invariance. It follows, only the s^*-wave component when coupled to $\langle \hat{c}^\dagger_{\mathbf{q}\sigma} \hat{c}_{\mathbf{q}\sigma} \rangle$ in Eq. (1.15) gives a non-null contribution, reducing the latter to

$$\begin{aligned}&\frac{2V}{L_x L_y} \sum_{\mathbf{q},\mathbf{q}'} \sum_\sigma \left[\cos(\delta q_x) + \cos(\delta q_y)\right] \langle \hat{c}^\dagger_{\mathbf{q}\sigma} \hat{c}_{\mathbf{q}\sigma} \rangle \hat{c}^\dagger_{\mathbf{q}'\sigma} \hat{c}_{\mathbf{q}'\sigma} \\ &\qquad = \frac{V}{L_x L_y} \sum_{\mathbf{q}'\sigma} \left(\cos q'_x + \cos q'_y\right) \hat{c}^\dagger_{\mathbf{q}'\sigma} \hat{c}_{\mathbf{q}'\sigma} \sum_{\mathbf{q}} \left(\cos q_x + \cos q_y\right) \langle \hat{c}^\dagger_{\mathbf{q}\sigma} \hat{c}_{\mathbf{q}\sigma} \rangle \qquad (1.16)\end{aligned}$$

Note that, for two vectors separated by a $\boldsymbol{\pi}$ shift,

$$\cos q_x + \cos q_y = -\cos(q_x + \pi) - \cos(q_y + \pi)$$

Because of this feature, changing the variables names $\mathbf{q}' \to \mathbf{k}$, $\mathbf{q} \to \mathbf{k}'$ for the sake of general aesthetic coherence, it becomes evident that the above equation gives the bands renormalization:

$$\begin{aligned}&\epsilon_{\mathbf{k}} \equiv -2t \left(\cos k_x + \cos k_y\right) \\ &\tilde{\epsilon}_{\mathbf{k}} \equiv \epsilon_{\mathbf{k}} + \left[\frac{1}{2L_x L_y} \sum_{\mathbf{k}'} \left(\cos k'_x + \cos k'_y\right) \langle \hat{c}^\dagger_{\mathbf{k}'\sigma} \hat{c}_{\mathbf{k}'\sigma} \rangle\right] \times 2V \left(\cos k_x + \cos k_y\right)\end{aligned}$$

Note that on the left-hand side $\tilde{\epsilon}_{\mathbf{k}}$ is independent of σ. To explain this, let:

$$w^{(\mathbf{0})}_\sigma \equiv \frac{1}{2L_x L_y} \sum_{\mathbf{k} \in \mathrm{BZ}} \left(\cos k_x + \cos k_y\right) \langle \hat{c}^\dagger_{\mathbf{k}\sigma} \hat{c}_{\mathbf{k}\sigma} \rangle$$

By simple symmetry considerations, it must be $\langle \hat{c}^\dagger_{\mathbf{k}\uparrow} \hat{c}_{\mathbf{k}\uparrow} \rangle = \langle \hat{c}^\dagger_{\mathbf{k}\downarrow} \hat{c}_{\mathbf{k}\downarrow} \rangle$ (as is later seen explicitly). Then,

$$w^{(\mathbf{0})}_\uparrow = w^{(\mathbf{0})}_\downarrow \equiv w^{(\mathbf{0})}$$

The computation can be simplified:

$$\begin{aligned}w^{(\mathbf{0})} &= \frac{1}{2L_x L_y} \sum_{\mathbf{k} \in \mathrm{BZ}} \left(\cos k_x + \cos k_y\right) \langle \hat{c}^\dagger_{\mathbf{k}\uparrow} \hat{c}_{\mathbf{k}\uparrow} \rangle \\ &= \frac{1}{2L_x L_y} \sum_{\mathbf{k} \in \mathrm{MBZ}} \left(\cos k_x + \cos k_y\right) \langle \hat{c}^\dagger_{\mathbf{k}\uparrow} \hat{c}_{\mathbf{k}\uparrow} - \hat{c}^\dagger_{\mathbf{k}+\boldsymbol{\pi}\uparrow} \hat{c}_{\mathbf{k}+\boldsymbol{\pi}\uparrow} \rangle \\ &= \frac{1}{2L_x L_y} \sum_{\mathbf{k} \in \mathrm{MBZ}} \left(\cos k_x + \cos k_y\right) \langle \hat{\Psi}^\dagger_{\mathbf{k}\uparrow} \tau^z \hat{\Psi}_{\mathbf{k}\uparrow} \rangle \\ &= -\frac{1}{4L_x L_y} \sum_{\mathbf{k} \in \mathrm{MBZ}} \left(\cos k_x + \cos k_y\right) \frac{\tilde{\epsilon}_{\mathbf{k}}}{\tilde{E}_{\mathbf{k}}} \left[f\left(-\tilde{E}_{\mathbf{k}}; \beta, \tilde{\mu}\right) - f\left(\tilde{E}_{\mathbf{k}}; \beta, \tilde{\mu}\right)\right] \qquad (1.17)\end{aligned}$$

where in the second passage the sign change is due to the presence of the structure factor, and in the fourth passage Eq. (1.6) and the relations (1.7) have been used. It follows, finally, that the hopping parameter gets effectively renormalized:

$$\tilde{t} \equiv t - w^{(\mathbf{0})} V \qquad (1.18)$$

The full effective MFT hamiltonian is spin-independent, then similarly the renormalized parameters cannot exhibit spin dependency. This justifies the fact that $\tilde{t}$ is spin-independent, and so is $\tilde{\epsilon}_{\mathbf{k}}$.

Off-diagonal terms. Consider the off-diagonal terms of Eq. (1.14). These contribute instead to the gap renormalization, being out of diagonal in the 2×2 hamiltonian matrix. Define $\mathbf{q}$, $\mathbf{q}'$ as in Fig. 1.2b, and rewrite

$$-\frac{2V}{L_x L_y}\sum_{\mathbf{K},\mathbf{k}}\sum_{\sigma}\left[\cos\left(2k_x\right)+\cos\left(2k_y\right)\right]\langle\hat{c}^{\dagger}_{\mathbf{K}+\mathbf{k}\sigma}\hat{c}_{\mathbf{K}+\mathbf{k}+\boldsymbol{\pi}\sigma}\rangle\hat{c}^{\dagger}_{\mathbf{K}-\mathbf{k}\sigma}\hat{c}_{\mathbf{K}-\mathbf{k}-\boldsymbol{\pi}\sigma}$$
$$=-\frac{2V}{L_x L_y}\sum_{\mathbf{q}}\langle\hat{c}^{\dagger}_{\mathbf{q}\sigma}\hat{c}_{\mathbf{q}+\boldsymbol{\pi}\sigma}\rangle\sum_{\mathbf{q}'\sigma}\left[\cos\left(\delta q_x\right)+\cos\left(\delta q_y\right)\right]\hat{c}^{\dagger}_{\mathbf{q}'\sigma}\hat{c}_{\mathbf{q}'+\boldsymbol{\pi}\sigma}$$

Identical considerations about the s^*-wave symmetry structure of the expectation value $\langle\hat{c}^{\dagger}_{\mathbf{q}\sigma}\hat{c}_{\mathbf{q}+\boldsymbol{\pi}\sigma}\rangle$ as in the above paragraph hold. Once again renaming the variables $\mathbf{q}' \to \mathbf{k}$, $\mathbf{q} \to \mathbf{k}'$ for the sake of general aesthetic coherence, this gives

$$-\frac{2V}{L_x L_y}\sum_{\mathbf{K},\mathbf{k}}\sum_{\sigma}\left[\cos\left(2k_x\right)+\cos\left(2k_y\right)\right]\langle\hat{c}^{\dagger}_{\mathbf{K}+\mathbf{k}\sigma}\hat{c}_{\mathbf{K}+\mathbf{k}+\boldsymbol{\pi}\sigma}\rangle\hat{c}^{\dagger}_{\mathbf{K}-\mathbf{k}\sigma}\hat{c}_{\mathbf{K}-\mathbf{k}-\boldsymbol{\pi}\sigma}$$
$$=-2V\left[\frac{1}{2L_x L_y}\sum_{\mathbf{k}'}\left(\cos k'_x+\cos k'_y\right)\langle\hat{c}^{\dagger}_{\mathbf{k}'\sigma}\hat{c}_{\mathbf{k}'+\boldsymbol{\pi}\sigma}\rangle\right]\sum_{\mathbf{k}\sigma}\left(\cos k_x+\cos k_y\right)\hat{c}^{\dagger}_{\mathbf{k}\sigma}\hat{c}_{\mathbf{k}+\boldsymbol{\pi}\sigma} \tag{1.19}$$

Because of this, the x component of the pseudo-magnetic field – the gap already renormalized by Eq. (1.11) when analyzing o.s. terms – takes up another renormalization contribution, finally giving

$$\tilde{\Delta}_{\mathbf{k}\sigma} \equiv m(U+2zV)\times(-1)^{\delta_{\sigma=\uparrow}} + i2Vw^{(\boldsymbol{\pi})}_{\sigma}\left(\cos k_x+\cos k_y\right) \tag{1.20}$$

where

$$w^{(\boldsymbol{\pi})}_{\sigma} \equiv -\frac{i}{2L_x L_y}\sum_{\mathbf{k}\in\mathrm{BZ}}\left(\cos k_x+\cos k_y\right)\langle\hat{c}^{\dagger}_{\mathbf{k}\sigma}\hat{c}_{\mathbf{k}+\boldsymbol{\pi}\sigma}\rangle$$

As will be clear in few lines, $w^{(\boldsymbol{\pi})}_{\sigma}$ as is defined here is purely real (due to the presence of a $-i$ prefactor). This makes $\tilde{\Delta}_{\mathbf{k}\sigma}$ made of two contributions,

$$\mathrm{Re}\{\tilde{\Delta}_{\mathbf{k}\sigma}\} = m(U+2zV)\times(-1)^{\delta_{\sigma=\uparrow}} \qquad \mathrm{Im}\{\tilde{\Delta}_{\mathbf{k}\sigma}\} = 2Vw^{(\boldsymbol{\pi})}_{\sigma}\left(\cos k_x+\cos k_y\right)$$

Now, since the gapped band value cannot depend on the spin index for symmetry reasons,

$$\tilde{E}_{\mathbf{k}} = \sqrt{\tilde{\epsilon}^2_{\mathbf{k}}+|\tilde{\Delta}_{\mathbf{k}\sigma}|^2}$$

this implies necessarily $|\tilde{\Delta}_{\mathbf{k}\uparrow}| = |\tilde{\Delta}_{\mathbf{k}\downarrow}|$. This is possible either if $w^{(\boldsymbol{\pi})}_{\uparrow} = \pm w^{(\boldsymbol{\pi})}_{\downarrow}$. Actually, in the end the exact sign does not matter: all that matters is the gap amplitude $|\tilde{\Delta}_{\mathbf{k}\sigma}|$, thus we may restrict to $\sigma =\uparrow$ and omit from now on the spin index. [Not so sure about this.]. This then gives us the final result for the renormalized gap function,

$$\tilde{\Delta}_{\mathbf{k}} \equiv m(U+2zV) + 2iw^{(\boldsymbol{\pi})}V\left(\cos k_x+\cos k_y\right) \tag{1.21}$$

This result, together with Eqns. (1.9) and (1.18), concludes the renormalization of all parameters due to the non-local interaction. To calculate $w^{(\boldsymbol{\pi})}$ self consistently, we may use:

$$\begin{aligned}
w^{(\boldsymbol{\pi})} &= -\frac{i}{2L_x L_y}\sum_{\mathbf{k}\in\mathrm{BZ}}\left(\cos k_x+\cos k_y\right)\langle\hat{c}^{\dagger}_{\mathbf{k}\uparrow}\hat{c}_{\mathbf{k}+\boldsymbol{\pi}\uparrow}\rangle \\
&= -\frac{i}{2L_x L_y}\sum_{\mathbf{k}\in\mathrm{MBZ}}\left(\cos k_x+\cos k_y\right)\langle\hat{c}^{\dagger}_{\mathbf{k}\uparrow}\hat{c}_{\mathbf{k}+\boldsymbol{\pi}\uparrow}-\hat{c}^{\dagger}_{\mathbf{k}+\boldsymbol{\pi}\uparrow}\hat{c}_{\mathbf{k}\uparrow}\rangle \\
&= \frac{1}{2L_x L_y}\sum_{\mathbf{k}\in\mathrm{MBZ}}\left(\cos k_x+\cos k_y\right)\langle\hat{\Psi}^{\dagger}_{\mathbf{k}\uparrow}\tau^y\hat{\Psi}_{\mathbf{k}\uparrow}\rangle \\
&= \frac{1}{4L_x L_y}\sum_{\mathbf{k}\in\mathrm{MBZ}}\left(\cos k_x+\cos k_y\right)\frac{\mathrm{Im}\{\tilde{\Delta}_{\mathbf{k}}\}}{\tilde{E}_{\mathbf{k}}}\left[f\left(-\tilde{E}_{\mathbf{k}};\beta,\tilde{\mu}\right)-f\left(\tilde{E}_{\mathbf{k}};\beta,\tilde{\mu}\right)\right]
\end{aligned} \tag{1.22}$$

Notice that this expression is purely real, as promised, and contributes to the y component of the pseudo-field of Fig. 1.1.

1.3.3 Renormalized hamiltonian behavior

Summing up, the non-local interaction $\hat{H}_V$ when discussed within MFT affects the EHM hamiltonian by renormalizing the various parameters as:

$$\begin{aligned}\tilde{\mu} &\equiv \mu + 2znV \\ \tilde{t} &\equiv t - w^{(\mathbf{0})}V \\ \tilde{\Delta}_{\mathbf{k}} &\equiv m(U + 2zV) + 2iw^{(\boldsymbol{\pi})}V\left[\cos\left(k_x\right) + \cos\left(k_y\right)\right]\end{aligned}$$

Various details are to be noted. First, the non-local interaction both contributes by enlarging the real part of the gap [To be understood: why does a non-local attraction increase the gap?] as well as introducing a s^*-wave shaped imaginary gap. Interestingly, if

$$\left(w^{(\mathbf{0})}\right)^{-1} = V/t$$

the diffusive part of the hamiltonian drops to zero. For even larger values, diffusion becomes energetically expensive and V-induced localization appears.

The new set of Hartree-Fock parameters to be determined is given by the vector

$$\mathbf{v} \equiv \begin{bmatrix} m \\ w^{(\mathbf{0})} \\ w^{(\boldsymbol{\pi})} \end{bmatrix}$$

Its three components are self-consistently determined by Eqns. (1.17) and (1.22). The self-consistent equation for m comes from Eq. (A.16), and reads

$$\begin{aligned} m &= \frac{1}{2L_xL_y}\sum_{\mathbf{k}\in\mathrm{BZ}}\langle\hat{c}^\dagger_{\mathbf{k}\uparrow}\hat{c}_{\mathbf{k}+\boldsymbol{\pi}\uparrow} - \hat{c}^\dagger_{\mathbf{k}\downarrow}\hat{c}_{\mathbf{k}+\boldsymbol{\pi}\downarrow}\rangle \\ &= \frac{1}{2L_xL_y}\sum_{\mathbf{k}\in\mathrm{MBZ}}\langle\hat{\Psi}^\dagger_{\mathbf{k}\uparrow}\tau^x\hat{\Psi}_{\mathbf{k}\uparrow} - \hat{\Psi}^\dagger_{\mathbf{k}\downarrow}\tau^x\hat{\Psi}_{\mathbf{k}\downarrow}\rangle \\ &= \frac{1}{L_xL_y}\sum_{\mathbf{k}\in\mathrm{MBZ}}\langle\hat{\Psi}^\dagger_{\mathbf{k}\uparrow}\tau^x\hat{\Psi}_{\mathbf{k}\uparrow}\rangle \\ &= \frac{1}{2L_xL_y}\sum_{\mathbf{k}\in\mathrm{MBZ}}\frac{\mathrm{Re}\{\tilde{\Delta}_{\mathbf{k}}\}}{\tilde{E}_{\mathbf{k}}}\left[f\left(-\tilde{E}_{\mathbf{k}};\beta,\tilde{\mu}\right) - f\left(\tilde{E}_{\mathbf{k}};\beta,\tilde{\mu}\right)\right] \end{aligned} \tag{1.23}$$

In the second passage $\langle\hat{\Psi}^\dagger_{\mathbf{k}\uparrow}\tau^x\hat{\Psi}_{\mathbf{k}\uparrow}\rangle = -\langle\hat{\Psi}^\dagger_{\mathbf{k}\downarrow}\tau^x\hat{\Psi}_{\mathbf{k}\downarrow}\rangle$ has been used. In the third passage, relations (1.7) were inserted. The algorithm sketched in Sec. A.3.7 remains essentially identical, with the *caveat* of defining three HF parameters, running for each a convergence analysis.

1.4 Stability of the AF phase

The discussion above is formally correct and self-consistent, thus a HF algorithm can be sketched to extract the HFPs. However we cannot proceed without considering the instability effects of Sec. A.3.6. As is known (and we would have liked to notice earlier) the AF-SSB at wavevector $\boldsymbol{\pi}$ we are studying here, responsible of halving the BZ down to the MBZ, can produce a stable phase on pure Hubbard lattices only at half filling [9]. For the EHM the situation is even worse than that: repeating the simple Linear Reponse Theory (LRT) computations of Sec. A.3.6 and mimicking Eq. (A.17), we get a proper response function

$$\tilde{\chi}_{\hat{\mathbf{S}}^-\hat{\mathbf{S}}^+}(\mathbf{k},\omega) = \frac{\chi_{\hat{\mathbf{S}}^-\hat{\mathbf{S}}^+}(\mathbf{k},\omega)}{1 - \left[U - 2V(\cos k_x + \cos k_y)\right]\chi_{\hat{\mathbf{S}}^-\hat{\mathbf{S}}^+}(\mathbf{k},\omega)} \tag{1.24}$$

[Double check the red part and conclude this paragraph...].

As is well documented in literature [10], AF can establish in a wide range of spatial structures with particular shapes, for example stripes. In order to extract the precise AF phase, we should

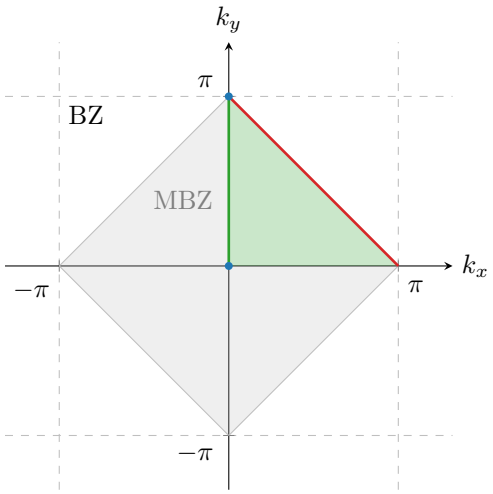

Color code	$w(\mathbf{k})$
White	0
Gray	0
Blue	1
Red	2
Green	4

Figure 1.3 | Graphic rendition of s^*-wave symmetry over the MBZ employed to optimize calculations. The right-side table indicates, for any point in BZ, the relative weight assigned to calculation.

1. Choose an initializer wavevector, say $\mathbf{k} = \boldsymbol{\pi}$;
2. Solve self-consistently for the HFPs at $\mathbf{k}$;
3. Compute the free energy F as a functional of the wavevector around $\mathbf{k}$;
4. Look for gradient descent of the free energy, $\boldsymbol{\nabla} F < 0$;
5. If the gradient descent is found, update $\mathbf{k} \to \mathbf{k} + \delta\mathbf{k}$ and repeat from step 2, otherwise halt.

Of course the sketched procedure can lead to a lot of complications, first the fact that at incommensurate wavevector $\mathbf{k} \neq \boldsymbol{\pi}$ the unit cell is not as simple as a pair of sites, but can become much larger requiring more refined computational solutions.

In this text we will show the self consistent result for AF-SSB at wavevector $\boldsymbol{\pi}$ even at finite doping as a first step in the above sketched procedure. The presented results are self-consistent, but unfortunately deeply unstable and unphysical at finite doping, a situation where an incommensurate and insulating AF phase is preferred to this commensurate metallic counterpart. Nevertheless we present them anyway.

1.5 HF algorithm, computational strategy and results

This section is devoted to the discussion of the self-consistent results we obtained running an iterative HF algorithm in the parameters space. As said earlier, not all presented results are in fact stable; however we decided to show them as sketch of the first step in a general self-consistent algorithm in search of the stablest AF structure.

1.5.1 Preliminary symmetry considerations

A very important feature when dealing with optimization is recognizing the complete s^* symmetry of the model, and the HFP parameters with relative self-consistency equations. Consider Eqns. (1.23), (1.17) and (1.22): in all of three the term inside the sum exhibits s^*-wave symmetry and is summed over the MBZ. Then there is no need of sweeping the entirety of the MBZ, it suffices to sweep just one fourth and just multiply coherently the result.

A little care is necessary when dealing with borders, due to MBZ nesting. Consider in fact the MBZ rhombus, sketched in gray in Fig. 1.3: due to periodicity, two of its four boundaries must be excluded from computation in order to avoid redundancy. Let those be the lower boundaries,

$$k_y = |k_x| - \pi$$

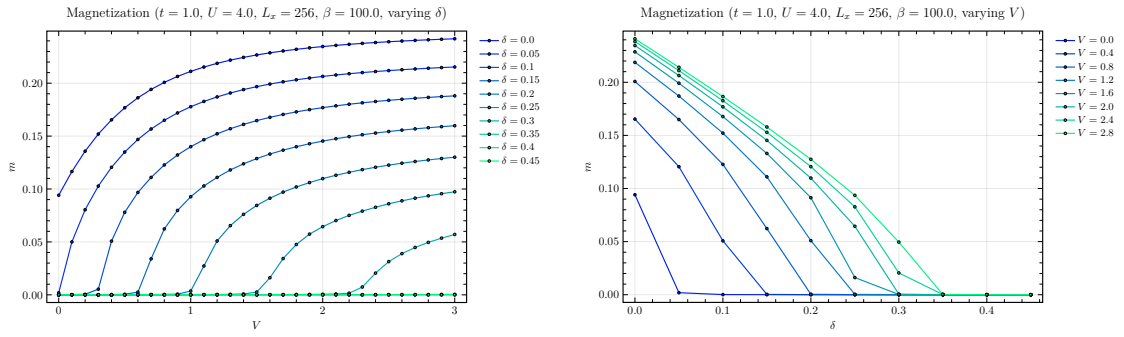

a | Non-local attraction V/t depencence.

b | Doping $\delta = n - 0.5$ dependence.

Figure 1.4 | Plots of the magnetization m in the antiferromagnetic phase as a function of both the non-local attraction V/t (Fig. 1.4a) and the doping $\delta = n - 1/2$ (Fig. 1.4b), at fixed local repulsion $U/t = 4$. As discussed in text, actually only $\delta = 0$ simulations are stable.

Due to periodicity, the remaining upper boundaries lead to identical results, thus we may compute just one of them and multiply the result by 2. In doing this, we need to avoid the edges: due to nesting of the MBZ, the three points

$$(0, \pi) \qquad (-\pi, 0) \qquad (\pi, 0)$$

are the same point. Thus these need to be considered once. Looking to the bulk of the rhombus, due to s^* periodicity it suffices to integrate over one quarter (considering just one internal border) and multiply by 4. In doing this, the origin $(0, 0)$ must be counted only once. Fig. 1.3 summarizes this argument: if we assign to any given point $\mathbf{k} \in \mathrm{BZ}$ a weight function $w(\mathbf{k})$ defined as in figure, in particular avoiding computations over white and gray points, we get an optimized integral over the entire MBZ saving *circa* 75% of runtime.

1.5.2 Results of the HF algorithm at generic doping

Within this section we will ignore stability considerations. The first set of simulations was run keeping the local repulsion fixed at a *not-so-strong* coupling value, $U/t = 4$, and letting V vary up to a comparable value, $0 \leq V/t \leq 3$, for various fillings. The temperature is kept to a finite large value $\beta = 100$ to avoid Fermi surface discontinuities, while lattice size is kept to a reasonably high value $L_x = L_y = 256$ to suppress finite-size effects while keeping runtime low enough. The HF has been set with the following parameters:

```
p::Int64 = 100                          # Maximum number of iterations
dv::Dict{String,Float64} = Dict([       # Relative tolerance on each HFP
    "m" => 1e-4,
    "w0" => 1e-4,
    "wp" => 1e-4
])
dn::Float64 = 1e-2                      # Relative tolerance on density
g::Float64 = 0.5                        # Mixing parameter
```

First HFP: m (magnetization). Consider first Fig. 1.4a. As is to be expected from Eq. (1.23), being it dependent on

$$\mathrm{Re}\{\tilde{\Delta}_{\mathbf{k}}\} = m(U + 2zV) \quad \text{with } z = 4$$

in this renormalized antiferromagnetic phase the non-local attraction acts as a magnetization boost, essentially reproducing the same behavior of m with U for the conventional Hubbard model plotted in Fig. A.6. The non-local attraction also enlarges the AF phase when considering various dopings,

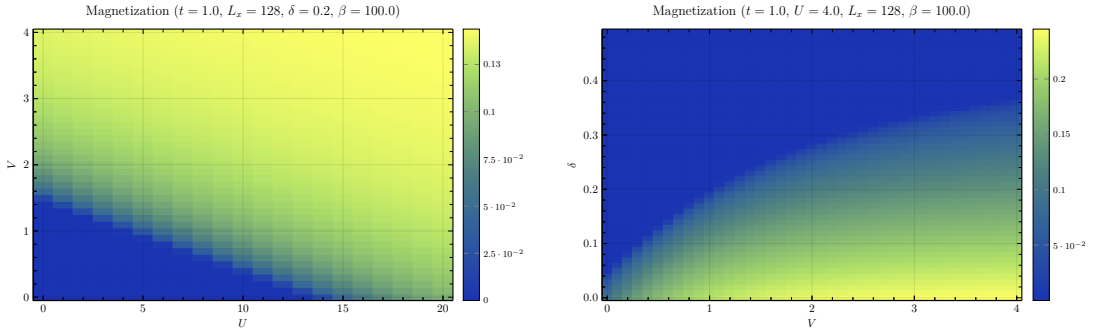

a | Magnetization in the UV plane.

b | Magnetization in the $V\delta$ plane.

Figure 1.5 | Heatmaps of the magnetization m in the antiferromagnetic phase in the UV plane (Fig. 1.5a) and the $V\delta$ plane (Fig. 1.5b).

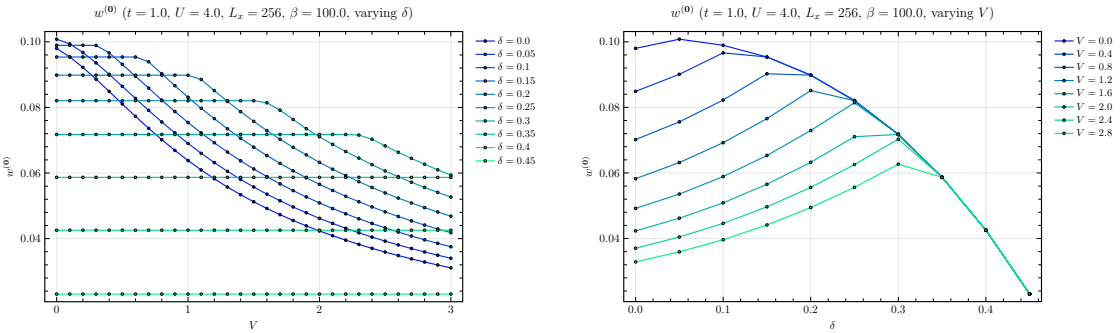

a | Non-local attraction V/t depencence.

b | Doping $\delta = n - 0.5$ dependence.

Figure 1.6 | Plots of the parameter $w^{(\mathbf{0})}$ in the antiferromagnetic phase as a function of both the non-local attraction V/t (Fig. 1.6a) and the doping $\delta = n - 1/2$ (Fig. 1.6b), at fixed local repulsion $U/t = 4$.

as is seen in Fig. 1.4. The magnetized region is largely extended with respect to the low-doped segment that magnetizes at $V = 0$. These effects are not particularly interesting or surprising. However, something more interesting arises when looking to Fig. 1.5, a couple of heatmaps in UV and $V\delta$ planes obtained respectively at $\delta = 0.2$ and $U = 4.0$, with L_x halved down to 128 for computational reasons. Fig. 1.5 expresses again the boost to magnetization given by V, with a magnetized region separated by a linear boundary approximately tilted as $-1/2z$, coherently with the renormalization of $\mathrm{Re}\{\tilde{\Delta}_{\mathbf{k}}\}$. Fig. 1.5b in particular is interesting: a sort of shallow "phase boundary" appears to follow a regular sub-linear curve.

Second HFP: $w^{(\mathbf{0})}$ (hopping renormalization coefficient). Moving to the second HFP, things get interesting. Fig. 1.6 is set up as Fig. 1.4, while Fig. 1.7 as Fig. 1.5. When considering the behavior of the parameter at fixed U, thus looking to Fig. 1.6a, a series of *plateaus* later interrupted by a continuous change in derivative are present at each doping. This is clearly evident also in Fig. 1.5b, with the parameter staying constant when approaching from left the maximum situated at the position of the "phase boundary" of Fig. 1.5b. The fact that there exists a geometric region of the $V\delta$ plane where are located both the phase transition and the maximum of this parameter, which controls hopping renormalization, is particularly interesting, suggesting the possibility of finding a maximally localized system by following the path extrapolated by maximizing $w^{(\mathbf{0})}$ around the phase transition.

Interestingly enough, the highly doped region, $\delta > 0.4$, presents seemingly no dependency on V in Fig. 1.7b (at least for thus value of U), as is also evident from the asymptotic behavior at increasing V visible in Fig. 1.7b. Moreover, Fig. 1.5a and 1.7a appear almost reciprocal: where one parameter grows, the other is suppressed. In terms of hopping renormalization, this tells us

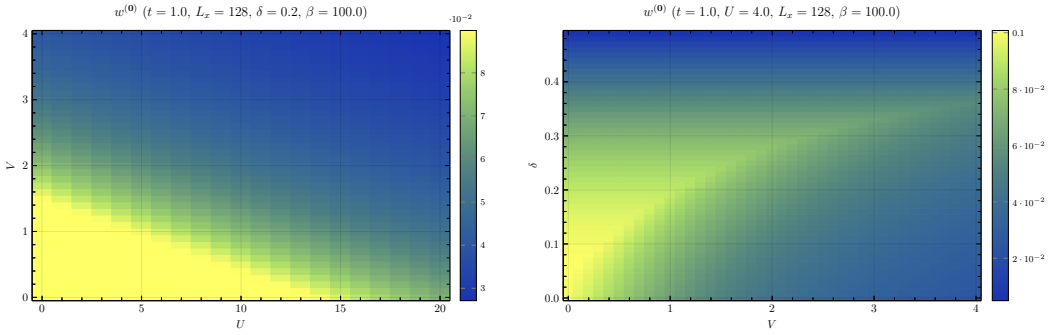

a | Magnetization in the UV plane. b | Magnetization in the $V\delta$ plane.

Figure 1.7 | Heatmaps of the parameter $w^{(\mathbf{0})}$ in the antiferromagnetic phase in the UV plane (Fig. 1.7a) and the $V\delta$ plane (Fig. 1.7b).

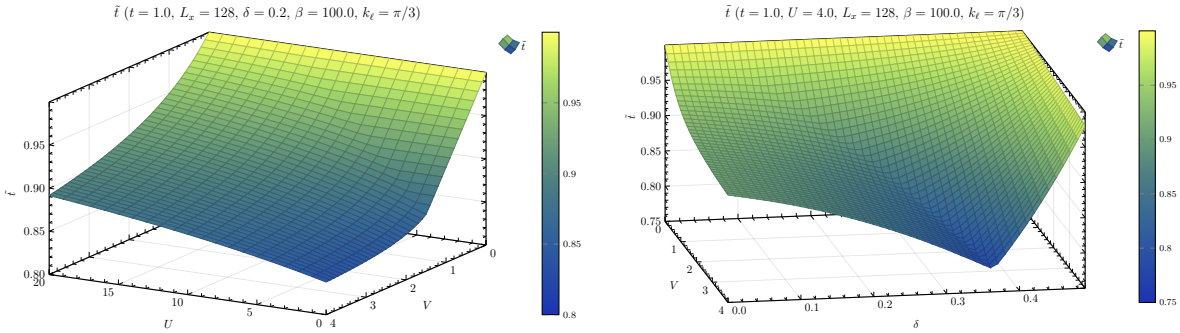

a | Effective hopping in the UV plane. b | Effective hopping in the $V\delta$ plane.

Figure 1.8 | Plots of the effective hopping $\tilde{t}$ in the antiferromagnetic phase in the UV plane (Fig. 1.8a) and the $V\delta$ plane (Fig. 1.8b).

that antiferromagnetic ordering tends to maintain t non-renormalized.

Fig. 1.8 reports in its subplots the renormalized hopping as a function of the model parameters, in the same setups as in the aforementioned heatmaps. As is depicted, the NN interaction V tends to reduce effective hopping amplitude down to a significant fraction of the starting value: t is damped of a 30% factor or so. As is evident from Fig. 1.8b, for a small local repulsion $U = 4$ the value of $\tilde{t}$ lowers as the doping grows, reaching a maximum approximately on the position of the maxima of $w^{(\mathbf{0})}$ in Fig. 1.7b, which was expected considering Eq. (1.18).

Third HFP: $w^{(\boldsymbol{\pi})}$ (imaginary gap coefficient). Unsurprisingly, the third HFP turns out to be essentially zero in all parameters space, considering also numerical fluctuations. This was expected: when deriving the MF solution to the model within AF phase, we essentially reduced it to the already known solution of Sec. A.3. The gap there was a real parameter, thus by purely renormalizing the parameters obtained within such solution there is no need for the present gap to acquire a non-zero imaginary part.

1.5.3 Role of hopping renormalization: switching off $w^{(\mathbf{0})}$

[To be continued...]

Appendix A

Mean-Field Theory in Hubbard lattices

In this Appendix the MFT solutions to the conventional Hubbard hamiltonian of Eq. (**??**),

$$\hat{H} = -t \sum_{\langle ij \rangle} \sum_{\sigma} \hat{c}^{\dagger}_{i\sigma} \hat{c}_{j\sigma} + U \sum_{i} \hat{n}_{i\uparrow} \hat{n}_{i\downarrow} \qquad t, U > 0 \tag{A.1}$$

are described. The discussion is limited to the two-dimensional square lattice.

A.1 Symmetries of the Hubbard model and magnetic phase transitions

The Hubbard model defined on the planar square lattice presents various natural symmetries, discussed in detail by Arovas et al. [1] and for the EHM in Sec. **??**. These are reported in Tab. **??**. For the conventional Hubbard model, $\hat{H}_t + \hat{H}_U$, the three essential symmetries are translational invariance, spin rotations and charge conservation. In this appendix we investigate magnetic ordering: thus we perform a SU(2) $\rightarrow$ U(1) SSB of the kind depicted in Fig. **??**, choosing a particular magnetization direction.

As is done in Chap. **??**, the starting point is to apply Wick's theorem to reduce the quartic hamiltonian of Eq. (A.1) to a quadratic form. Considering the discussion that leads to Eq. (**??**), it's evident that for the symmetry scheme we are dealing with the Fock term in decomposition is always suppressed, as well as the Cooper term. Then we remain with just the Hartree term,

$$\begin{aligned} \hat{n}_{i\uparrow} \hat{n}_{i\downarrow} &= \left(\langle \hat{n}_{i\uparrow} \rangle + \delta \hat{n}_{i\uparrow} \right) \left(\langle \hat{n}_{i\downarrow} \rangle + \delta \hat{n}_{i\downarrow} \right) \\ &\simeq \langle \hat{n}_{i\uparrow} \rangle \langle \hat{n}_{i\downarrow} \rangle + \delta \hat{n}_{i\uparrow} \langle \hat{n}_{i\downarrow} \rangle + \langle \hat{n}_{i\uparrow} \rangle \delta \hat{n}_{i\downarrow} + \mathcal{O}\left(\delta n^2 \right) \\ &= - \langle \hat{n}_{i\uparrow} \rangle \langle \hat{n}_{i\downarrow} \rangle + \hat{n}_{i\uparrow} \langle \hat{n}_{i\downarrow} \rangle + \langle \hat{n}_{i\uparrow} \rangle \hat{n}_{i\downarrow} + \mathcal{O}\left(\delta n^2 \right) \end{aligned}$$

where $\delta \hat{n}_{i\sigma} \equiv \hat{n}_{i\sigma} - \langle \hat{n}_{i\sigma} \rangle$ and orders higher than first have been ignored, assuming negligible fluctuations around the equilibrium single-site population. The first term of the above three can be neglected at fixed particles number, being a pure energy shift.

A.2 Ferromagnetic phase

The MFT ferromagnetic solution prescribes an uniformly magnetized lattice,

$$\langle \hat{n}_{i\uparrow} \rangle = n + m \qquad \langle \hat{n}_{i\downarrow} \rangle = n - m$$

where n is the site electron density and m is the density unbalance, leading to a magnetization per site $2m$. The mean-field hamiltonian with these substitutions becomes:

$$\begin{aligned} \hat{H} &\simeq -t \sum_{\langle ij \rangle} \sum_{\sigma} \hat{c}^{\dagger}_{i\sigma} \hat{c}_{j\sigma} + U \sum_{i} \left[\hat{n}_{i\uparrow} \langle \hat{n}_{i\downarrow} \rangle + \langle \hat{n}_{i\uparrow} \rangle \hat{n}_{i\downarrow} \right] \\ &= -t \sum_{\langle ij \rangle} \sum_{\sigma} \hat{c}^{\dagger}_{i\sigma} \hat{c}_{j\sigma} + nU \sum_{i} \left[\hat{n}_{i\uparrow} + \hat{n}_{i\downarrow} \right] - mU \sum_{i} \left[\hat{n}_{i\uparrow} - \hat{n}_{i\downarrow} \right] \end{aligned}$$

Figure A.1 | Depiction of the Hubbard square lattice hopping band $\epsilon_{\mathbf{k}} = -2t[\cos(k_x) + \cos(k_y)]$. The red lines mark the zero-energy intersection.

Fourier transforming,

$$-t \sum_{\langle ij \rangle} \sum_{\sigma} \hat{c}^{\dagger}_{i\sigma} \hat{c}_{j\sigma} = -2t \sum_{\mathbf{k}\sigma} \left[\cos(k_x) + \cos(k_y)\right] \hat{n}_{\mathbf{k}\sigma}$$
$$nU \sum_{i} \left[\hat{n}_{i\uparrow} + \hat{n}_{i\downarrow}\right] = nU \sum_{\mathbf{k}\sigma} \hat{n}_{\mathbf{k}\sigma}$$
$$mU \sum_{i} \left[\hat{n}_{i\uparrow} - \hat{n}_{i\downarrow}\right] = mU \sum_{\mathbf{k}\sigma} \left[\hat{n}_{\mathbf{k}\uparrow} - \hat{n}_{\mathbf{k}\downarrow}\right]$$

For a square lattice, the Brillouin Zone is delimited by

$$\mathbf{k} \in [-\pi, \pi] \times [-\pi, \pi]$$

The hopping single-state energy is given by

$$\epsilon_{\mathbf{k}} = -2t \left[\cos(k_x) + \cos(k_y)\right]$$

represented as a band in Fig. A.1. At $U = 0$, the mean-field ferromagnetic state fills the band bottom-up. The single-state energy becomes:

$$\epsilon_{\mathbf{k}\uparrow} = U\,(n - m) - 2t \left[\cos(k_x) + \cos(k_y)\right]$$
$$\epsilon_{\mathbf{k}\downarrow} = U\,(n + m) - 2t \left[\cos(k_x) + \cos(k_y)\right]$$

Now it is a matter of finding the optimal value for m, minimizing the total energy at fixed filling $\rho = 2n$. Notice that said minimization is performed parametrically varying the magnetization m, inside the ferromagnetic-polarized space. As it turns out, for strong local repulsion $U/t \gg 1$, antiferromagnetic ordering is preferred. Comparison is needed in order to assess which magnetic ordering is preferred.

Consider the half-filling situation. An unpolarized system will have $n = 1/4$, $m = 0$: this implies $\langle \hat{n}_{i\uparrow} \rangle = \langle \hat{n}_{i\downarrow} \rangle = 1/4$. A perfectly up-ferromagnetic system, $n = 1/4$, $m = 1/4$: then $\langle \hat{n}_{i\uparrow} \rangle = 1/2$ and $\langle \hat{n}_{i\downarrow} \rangle = 0$. [To be continued...]

A.3 Antiferromagnetic phase

Consider now an AF mean-field solution. Let us change notation, indicating each site as

$$i \to \mathbf{r} = (x, y) \qquad x, y \in \mathbb{N}$$

The mean-field AF solution at half-filling is the uniform-modulated magnetization

$$m_{\mathbf{r}} = (-1)^{x+y} m \qquad m \in [-1, 1]$$

and a mean-field Ansatz

$$\langle \hat{n}_{\mathbf{r}\uparrow} \rangle = n + m_{\mathbf{r}} \qquad \langle \hat{n}_{\mathbf{r}\downarrow} \rangle = n - m_{\mathbf{r}} \tag{A.2}$$

In next sections, the details of the MFT solution are discussed.

A.3.1 MFT discussion

With respect to the ferromagnetic solution presented above, the only detail changing is the last term,

$$\hat{H} = -t \sum_{\langle \mathbf{r}\mathbf{r}' \rangle} \sum_{\sigma} \hat{c}^{\dagger}_{\mathbf{r}\sigma} \hat{c}_{\mathbf{r}'\sigma} + nU \sum_{\mathbf{r}} \left[\hat{n}_{\mathbf{r}\uparrow} + \hat{n}_{\mathbf{r}\downarrow}\right] - mU \sum_{\mathbf{r}} (-1)^{x+y} \left[\hat{n}_{\mathbf{r}\uparrow} - \hat{n}_{\mathbf{r}\downarrow}\right] \tag{A.3}$$

Figure A.2 | Alternative depiction of the Hubbard square lattice hopping band previously reported in Fig. A.1. The Magnetic Brillouin Zone (MBZ) is delimited by the zero-energy contour and is indicated in figure. As it is evident, energy sign flips by taking a (π, π) translation in $\mathbf{k}$ space.

Fourier-transforming, the phase factor can be absorbed in the destruction operator inside of $\hat{n}_{\mathbf{r}\sigma}$:

$$\begin{aligned}\sum_{\mathbf{r}}(-1)^{x+y}\hat{n}_{\mathbf{r}\sigma} &= \sum_{\mathbf{r}}(-1)^{x+y}\hat{c}^{\dagger}_{\mathbf{r}\sigma}\hat{c}_{\mathbf{r}\sigma}\\ &= \sum_{\mathbf{r}} e^{i\boldsymbol{\pi}\cdot\mathbf{r}}\frac{1}{\sqrt{L_xL_y}}\sum_{\mathbf{k}\in\mathrm{BZ}} e^{i\mathbf{k}\cdot\mathbf{r}}\hat{c}^{\dagger}_{\mathbf{k}\sigma}\frac{1}{\sqrt{L_xL_y}}\sum_{\mathbf{k}'\in\mathrm{BZ}} e^{-i\mathbf{k}'\cdot\mathbf{r}}\hat{c}_{\mathbf{k}'\sigma}\\ &= \sum_{\mathbf{k}\in\mathrm{BZ}}\sum_{\mathbf{k}'\in\mathrm{BZ}}\hat{c}^{\dagger}_{\mathbf{k}\sigma}\hat{c}_{\mathbf{k}'\sigma}\frac{1}{L_xL_y}\sum_{\mathbf{r}} e^{-i[\mathbf{k}'-(\mathbf{k}+\boldsymbol{\pi})]\cdot\mathbf{r}}\\ &= \sum_{\mathbf{k}\in\mathrm{BZ}}\hat{c}^{\dagger}_{\mathbf{k}\sigma}\hat{c}_{\mathbf{k}+\boldsymbol{\pi}\sigma}\end{aligned}$$

where $\boldsymbol{\pi} = (\pi, \pi)$. It follows:

$$mU\sum_{\mathbf{r}}(-1)^{x+y}\left[\hat{n}_{\mathbf{r}\uparrow} - \hat{n}_{\mathbf{r}\downarrow}\right] = \Delta\sum_{\mathbf{k}\in\mathrm{BZ}}\left[\hat{c}^{\dagger}_{\mathbf{k}\uparrow}\hat{c}_{\mathbf{k}+\boldsymbol{\pi}\uparrow} - \hat{c}^{\dagger}_{\mathbf{k}\downarrow}\hat{c}_{\mathbf{k}+\boldsymbol{\pi}\downarrow}\right] \quad \text{where} \quad \Delta \equiv mU$$

Consider the band of Fig. A.1 at half-filling. As does Fabrizio [4], the area delimited externally by the solid lines at zero energy is denominated "Magnetic Brillouin Zone" (MBZ). The periodicity of $\mathbf{k}$ space guarantees that the full BZ can be taken as well to be the one of Fig. **??**. Then:

$$\begin{aligned}\sum_{\mathbf{k}\in\mathrm{BZ}}\hat{c}^{\dagger}_{\mathbf{k}\uparrow}\hat{c}_{\mathbf{k}+\boldsymbol{\pi}\uparrow} &= \sum_{\mathbf{k}\in\mathrm{MBZ}}\left[\hat{c}^{\dagger}_{\mathbf{k}\uparrow}\hat{c}_{\mathbf{k}+\boldsymbol{\pi}\uparrow} + \hat{c}^{\dagger}_{\mathbf{k}+\boldsymbol{\pi}\uparrow}\hat{c}_{\mathbf{k}+2\boldsymbol{\pi}\uparrow}\right]\\ &= \sum_{\mathbf{k}\in\mathrm{MBZ}}\left[\hat{c}^{\dagger}_{\mathbf{k}\uparrow}\hat{c}_{\mathbf{k}+\boldsymbol{\pi}\uparrow} + \hat{c}^{\dagger}_{\mathbf{k}+\boldsymbol{\pi}\uparrow}\hat{c}_{\mathbf{k}\uparrow}\right]\end{aligned} \tag{A.4}$$

and the same applies for spin $\downarrow$. Periodicity by shifts $2\boldsymbol{\pi}$ has been used. Now, define the Nambu spinors:

$$\hat{\Psi}_{\mathbf{k}\sigma} \equiv \begin{bmatrix}\hat{c}_{\mathbf{k}\sigma}\\ \hat{c}_{\mathbf{k}+\boldsymbol{\pi}\sigma}\end{bmatrix}$$

and a spin-wise gap,

$$\Delta_{\uparrow} = \Delta \qquad \Delta_{\downarrow} = -\Delta$$

At fixed filling, the nU term is a pure chemical potential shift, thus will be neglected. The kinetic term transforms as

$$\begin{aligned}-t\sum_{\langle ij\rangle}\sum_{\sigma}\hat{c}^{\dagger}_{i\sigma}\hat{c}_{j\sigma} &= \sum_{\mathbf{k}\in\mathrm{BZ}}\sum_{\sigma}\epsilon_{\mathbf{k}}\hat{c}^{\dagger}_{\mathbf{k}\sigma}\hat{c}_{\mathbf{k}\sigma}\\ &= \sum_{\mathbf{k}\in\mathrm{MBZ}}\sum_{\sigma}\left[\epsilon_{\mathbf{k}}\hat{c}^{\dagger}_{\mathbf{k}\sigma}\hat{c}_{\mathbf{k}\sigma} + \epsilon_{\mathbf{k}+\boldsymbol{\pi}}\hat{c}^{\dagger}_{\mathbf{k}+\boldsymbol{\pi}\sigma}\hat{c}_{\mathbf{k}+\boldsymbol{\pi}\sigma}\right]\\ &= \sum_{\mathbf{k}\in\mathrm{MBZ}}\sum_{\sigma}\epsilon_{\mathbf{k}}\left[\hat{c}^{\dagger}_{\mathbf{k}\sigma}\hat{c}_{\mathbf{k}\sigma} - \hat{c}^{\dagger}_{\mathbf{k}+\boldsymbol{\pi}\sigma}\hat{c}_{\mathbf{k}+\boldsymbol{\pi}\sigma}\right]\end{aligned}$$

In the second passage, the sum over the full BZ was written considering that the entirety of the zone is given by all the points in the MBZ plus their conjugates obtained by a $\boldsymbol{\pi}$ shift in the flipped band. As depicted in Fig. **??**, kinetic energy is anti-periodic in $\mathbf{k}$ space by a vector $\boldsymbol{\pi}$. This anti-periodicity accounts for the minus sign arising in the third passage. The hamiltonian is then given by:

$$\hat{H} = \sum_{\mathbf{k}\in\mathrm{MBZ}}\sum_{\sigma}\hat{\Psi}^{\dagger}_{\mathbf{k}\sigma}h_{\mathbf{k}\sigma}\hat{\Psi}_{\mathbf{k}\sigma} \quad \text{being} \quad h_{\mathbf{k}\sigma} \equiv \begin{bmatrix}\epsilon_{\mathbf{k}} & -\Delta_{\sigma}\\ -\Delta_{\sigma} & -\epsilon_{\mathbf{k}}\end{bmatrix} \tag{A.5}$$

Notice: the Nambu hamiltonian is a 2×2 matrix over the MBZ – which is half the full BZ, coherently with a solution which essentially bipartites the lattice giving back a double sized unit cell.

Figure A.3 | Pseudo-magnetic field originating from mean-field treatment of the square Hubbard hamiltonian. Here, only the $\sigma =\uparrow$ situation is plotted.

Figure A.4 | Depiction of the AF bands $\pm E_{\mathbf{k}}$. [To be continued...]

A.3.2 Diagonalization and AF ground state

The system ground-state is obtained by the means of a Bogoliubov rotation. The hamiltonian maps onto the simple one of a spin in a magnetic field,

$$h_{\mathbf{k}\sigma} = \epsilon_{\mathbf{k}}\tau^z - \Delta_\sigma \tau^x$$

being τ^α the Pauli matrices. Then, defining

$$\hat{s}^\alpha_{\mathbf{k}\sigma} \equiv \hat{\Psi}^\dagger_{\mathbf{k}\sigma}\tau^\alpha\hat{\Psi}_{\mathbf{k}\sigma} \quad \text{and} \quad \mathbf{b}_{\mathbf{k}\sigma} \equiv \begin{bmatrix} -\Delta_\sigma \\ 0 \\ \epsilon_{\mathbf{k}} \end{bmatrix}$$

one gets:

$$\hat{H} = \sum_{\mathbf{k}\in\mathrm{MBZ}}\sum_\sigma \mathbf{b}_{\mathbf{k}\sigma}\cdot\hat{\mathbf{s}}_{\mathbf{k}\sigma} \quad \text{where} \quad \hat{\mathbf{s}}_{\mathbf{k}\sigma} = \begin{bmatrix} \hat{s}^x_{\mathbf{k}\sigma} \\ \hat{s}^y_{\mathbf{k}\sigma} \\ \hat{s}^z_{\mathbf{k}\sigma} \end{bmatrix} \tag{A.6}$$

The hamiltonian represents a system of spins subject to local magnetic fields, each tilted by an angle $\tan(2\theta_{\mathbf{k}\sigma}) = \Delta_\sigma/\epsilon_{\mathbf{k}}$, as sketched in Fig. A.3. At any finite temperature, the ground-state of such a system is well-known. Diagonalization of each $h_{\mathbf{k}\sigma}$ is obtained trivially by a simple rotation around the y axis:

$$d_{\mathbf{k}\sigma} = W_{\mathbf{k}\sigma}h_{\mathbf{k}\sigma}W^\dagger_{\mathbf{k}\sigma}$$

where

$$d_{\mathbf{k}\sigma} = \begin{bmatrix} -E_{\mathbf{k}} & \\ & E_{\mathbf{k}} \end{bmatrix} \quad \text{and} \quad W_{\mathbf{k}\sigma} = \exp\left\{ i\frac{2\theta_{\mathbf{k}\sigma}-\pi}{2}\tau^y \right\}$$

Note that rotation is taken to be of an angle $2\theta_{\mathbf{k}\sigma} - \pi$ in order to anti-align the pseudo-spin with the magnetic field of Fig. A.3 and thus order the eigenvalues as in $d_{\mathbf{k}\sigma}$, with the smaller one in the top-left corner of the matrix and the larger one in the bottom-right corner. The explicit form of the transformation matrix is thus

$$W_{\mathbf{k}\sigma} = \begin{bmatrix} \cos\theta_{\mathbf{k}\sigma} & -\sin\theta_{\mathbf{k}\sigma} \\ \sin\theta_{\mathbf{k}\sigma} & \cos\theta_{\mathbf{k}\sigma} \end{bmatrix}\begin{bmatrix} & -1 \\ 1 & \end{bmatrix} = \begin{bmatrix} -\sin\theta_{\mathbf{k}\sigma} & -\cos\theta_{\mathbf{k}\sigma} \\ \cos\theta_{\mathbf{k}\sigma} & -\sin\theta_{\mathbf{k}\sigma} \end{bmatrix} \tag{A.7}$$

Eigenvalues are:

$$E_{\mathbf{k}} \equiv \sqrt{\epsilon^2_{\mathbf{k}} + |\Delta_\sigma|^2} \tag{A.8}$$

Note that considering the full hamiltonian $\hat{H} - \mu\hat{N}$, the diagonalizing matrix remains the same, being

$$-\mu\hat{N} = \sum_{\mathbf{k}\in\mathrm{MBZ}}\begin{bmatrix} -\mu & \\ & -\mu \end{bmatrix} \quad \Longrightarrow \quad W_{\mathbf{k}\sigma}\left[h_{\mathbf{k}\sigma} - \mu\mathbb{I}_{2\times2}\right]W^\dagger_{\mathbf{k}\sigma} = d_{\mathbf{k}\sigma} - \mu\mathbb{I}_{2\times2} \tag{A.9}$$

thus for non-null chemical potential (i.e. finite doping) the eigenvalues are just shifted, $\pm E_{\mathbf{k}} - \mu$. In other words, the new bands retain the same chemical potential of the bare bands. Notice also that the presence of an absolute value makes the eigenvalues independent of the σ index. Eigenvector fermion operators are obtained simply as:

$$\hat{\Gamma}_{\mathbf{k}\sigma} = W_{\mathbf{k}\sigma}\hat{\Psi}_{\mathbf{k}\sigma} \tag{A.10}$$

The $\hat{\Gamma}$ spinor operators are effectively free fermionic spinor fields and as such must be treated.

The consequence of Eq. (A.9) is interesting by itself: within this HF solution, the gap opens always at $E = 0$. In other words, the bands sketched in Fig. A.4 retain the same geometric features

regardless of the doping, what changes is the bands width and the gap between them. The very key point here is that, being the two bands symmetric (thus containing each half of the electronic states) and defined over the MBZ, any finite doping $\delta > 0$ will produce a metallic behaviour, imposing that the chemical potential crosses the upper band. It is widely observed and confirmed by more refined numerical procedures, however, that AF establishes an insulating phase – here only reproduced at half-filling, where the chemical potential lies within the gap. As will be detailed in A.3.6, the commensurate nature of AF SSB at wavevector $\boldsymbol{\pi}$ of this self-consistent solution is highly unstable and atypical at finite doping [9].

A.3.3 Chemical potential and system density

The total number of electrons is given by

$$\begin{aligned} N &= \sum_{\mathbf{k}\sigma} \langle \hat{n}_{\mathbf{k}\sigma} \rangle \\ &= \sum_{\sigma} \sum_{\mathbf{k}\in \mathrm{MBZ}} \langle \hat{n}_{\mathbf{k}\sigma} + \hat{n}_{\mathbf{k}+\boldsymbol{\pi}\sigma} \rangle \\ &= \sum_{\sigma} \sum_{\mathbf{k}\in \mathrm{MBZ}} \left\langle \hat{\Gamma}^{\dagger}_{\mathbf{k}\sigma} \hat{\Gamma}_{\mathbf{k}\sigma} \right\rangle \\ &= 2 \sum_{\mathbf{k}\in \mathrm{MBZ}} \left[f\left(-E_{\mathbf{k}}; \beta, \mu\right) + f\left(E_{\mathbf{k}}; \beta, \mu\right) \right] \end{aligned} \tag{A.11}$$

being f be the Fermi-Dirac distribution at inverse temperature β and chemical potential μ,

$$f(\epsilon; \beta, \mu) = \frac{1}{e^{\beta(\epsilon-\mu)} + 1}$$

The 2 prefactor appeared because of spin degeneracy. Since the gapped bands refer to the smaller MBZ, thus exhibit the periodicity

$$E_{\mathbf{k}} = E_{\mathbf{k}+\boldsymbol{\pi}}$$

it holds equivalently

$$N = \sum_{\mathbf{k}\in \mathrm{BZ}} \left[f\left(-E_{\mathbf{k}}; \beta, \mu\right) + f\left(E_{\mathbf{k}}; \beta, \mu\right) \right] \tag{A.12}$$

as is obvious. The 2 prefactor was absorbed in doubling the integration region, MBZ $\to$ BZ. Next sections are devoted to simplify the above theoretical results in order to obtain an algorithmic estimation for the magnetization m, which is just the AF instability order parameter.

In Fig. A.5 the density $n(\mu)$ is plotted as a function of μ. As is evident, at nearly zero temperature ($\beta \to \infty$) the system is half filled for $-\Delta < \mu < \Delta$. In order to obtain a finite doping, it must be $|\mu| > \Delta$; which means, the chemical potential needs to cross the electronic bands. This HF solution leads invariably to a rather unusual metallic AF at any finite doping.

A.3.4 Self-consistent magnetization

A convergence algorithm can be designed to find the Hartree-Fock solution to the model. Ultimately, we aim to extract m self-consistently. Since

$$\begin{aligned} m &= \frac{1}{2L_xL_y} \sum_{\mathbf{r}} (-1)^{x+y} \langle \hat{n}_{\mathbf{r}\uparrow} - \hat{n}_{\mathbf{r}\downarrow} \rangle \\ &= \frac{1}{2L_xL_y} \sum_{\mathbf{k}\in \mathrm{BZ}} \left\langle \hat{c}^{\dagger}_{\mathbf{k}\uparrow} \hat{c}_{\mathbf{k}+\boldsymbol{\pi}\uparrow} - \hat{c}^{\dagger}_{\mathbf{k}\downarrow} \hat{c}_{\mathbf{k}+\boldsymbol{\pi}\downarrow} \right\rangle \\ &= \frac{1}{2L_xL_y} \sum_{\mathbf{k}\in \mathrm{MBZ}} \left\langle \left(\hat{c}^{\dagger}_{\mathbf{k}\uparrow} \hat{c}_{\mathbf{k}+\boldsymbol{\pi}\uparrow} + \hat{c}^{\dagger}_{\mathbf{k}+\boldsymbol{\pi}\uparrow} \hat{c}_{\mathbf{k}\uparrow} \right) - \left(\hat{c}^{\dagger}_{\mathbf{k}\downarrow} \hat{c}_{\mathbf{k}+\boldsymbol{\pi}\downarrow} + \hat{c}^{\dagger}_{\mathbf{k}+\boldsymbol{\pi}\downarrow} \hat{c}_{\mathbf{k}\downarrow} \right) \right\rangle \end{aligned}$$

In the last passage, Eq. (A.4) has been used. Then magnetization can be computed simply as

$$m = \frac{1}{2L_xL_y} \sum_{\mathbf{k}\in \mathrm{MBZ}} \left[\left\langle \hat{\Psi}^{\dagger}_{\mathbf{k}\uparrow} \tau^x \hat{\Psi}_{\mathbf{k}\uparrow} \right\rangle - \left\langle \hat{\Psi}^{\dagger}_{\mathbf{k}\downarrow} \tau^x \hat{\Psi}_{\mathbf{k}\downarrow} \right\rangle \right] \tag{A.13}$$

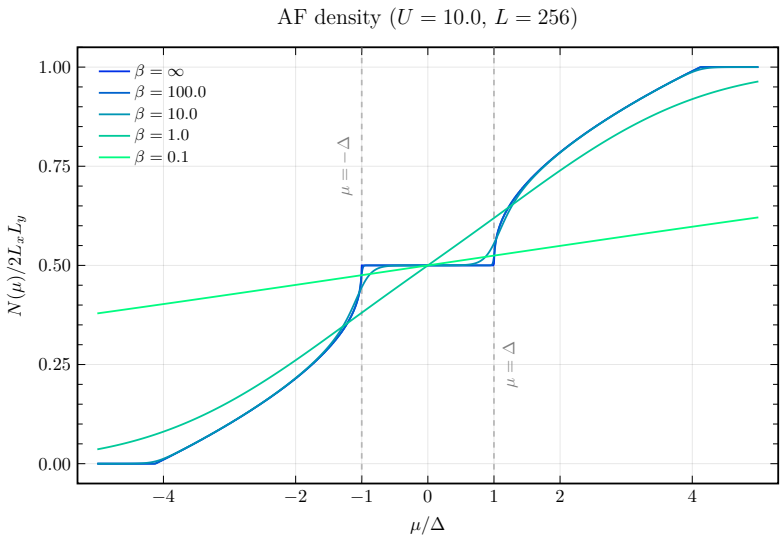

Figure A.5 | Electronic density in the AF phase as a function of the chemical potential, measured in relation to the gap Δ, at various temperatures.

In this equation, spin expectation values appear:

$$\left\langle \hat{\Psi}^\dagger_{\mathbf{k}\sigma} \tau^x \hat{\Psi}_{\mathbf{k}\sigma} \right\rangle = \langle \hat{s}^x_{\mathbf{k}\sigma} \rangle$$

Now discussion is divided in two parts: zero temperature and finite temperature.

Zero temperature solution. For a spin system at zero temperature, the spin operator expectation value anti-aligns with the external field,

$$\langle \hat{s}^x_{\mathbf{k}\sigma} \rangle = \sin(2\theta_{\mathbf{k}\sigma})$$

(see Fig. A.3). Now, since $\Delta_\downarrow = -\Delta_\uparrow$, it follows

$$\theta_{\mathbf{k}\uparrow} = -\theta_{\mathbf{k}\downarrow} \equiv \theta_{\mathbf{k}}$$

Then, from Eq. (A.13)

$$\begin{aligned} m &= \frac{1}{L_x L_y} \sum_{\mathbf{k}\in \mathrm{MBZ}} \sin(2\theta_{\mathbf{k}}) \\ &= \frac{1}{2L_x L_y} \sum_{\mathbf{k}\in \mathrm{BZ}} \sin(2\theta_{\mathbf{k}}) \end{aligned}$$

The last passage is due to the fact that the sum over the MBZ can be performed identically over BZ $\setminus$ MBZ and yield the same result. This is because of the lattice periodicity in reciprocal space. Then, finally:

$$m = \frac{1}{L_x L_y} \sum_{\mathbf{k}\in \mathrm{BZ}} [W_{\mathbf{k}\uparrow}]_{11} [W^\dagger_{\mathbf{k}\uparrow}]_{21} \tag{A.14}$$

where $\sin(2\theta_{\mathbf{k}}) = 2\sin\theta_{\mathbf{k}} \cos\theta_{\mathbf{k}}$ has been used. As will become clear in next section, the sudden appearance of matrix elements of W is not casual.

Finite temperature solution. At finite temperature β, discussion is analogous to the section above. Here will be treated somewhat more theoretically. Define the generic order parameter:

$$\Delta_{ij}(\mathbf{k}\sigma) \equiv \left\langle [\hat{\Psi}^\dagger_{\mathbf{k}\sigma}]_i [\hat{\Psi}_{\mathbf{k}\sigma}]_j \right\rangle$$

In last section, the relevant indices (i, j) were $(1, 2)$ and $(2, 1)$. Transform this order parameter,

$$\begin{aligned}
\Delta_{ij}(\mathbf{k}\sigma) &= \sum_{i'j'} \left\langle [\hat{\Gamma}^\dagger_{\mathbf{k}\sigma}]_{i'} [W_{\mathbf{k}\sigma}]_{i'i} [W^\dagger_{\mathbf{k}\sigma}]_{jj'} [\hat{\Gamma}_{\mathbf{k}\sigma}]_{j'} \right\rangle \\
&= \sum_{i'j'} [W_{\mathbf{k}\sigma}]_{i'i} [W^\dagger_{\mathbf{k}\sigma}]_{jj'} \left\langle [\hat{\Gamma}^\dagger_{\mathbf{k}\sigma}]_{i'} [\hat{\Gamma}_{\mathbf{k}\sigma}]_{j'} \right\rangle \\
&= \sum_{i'j'} [W_{\mathbf{k}\sigma}]_{i'i} [W^\dagger_{\mathbf{k}\sigma}]_{jj'} \delta_{i'j'} f\left([d_{\mathbf{k}\sigma}]_{i'i'}; \beta, \mu\right) \\
&= \sum_{\ell=1}^{2} [W_{\mathbf{k}\sigma}]_{\ell i} [W^\dagger_{\mathbf{k}\sigma}]_{j\ell} f\left((-1)^\ell E_{\mathbf{k}\sigma}; \beta, \mu\right) \\
&= [W_{\mathbf{k}\sigma}]_{1i} [W^\dagger_{\mathbf{k}\sigma}]_{j1} f\left(-E_{\mathbf{k}}; \beta, \mu\right) + [W_{\mathbf{k}\sigma}]_{2i} [W^\dagger_{\mathbf{k}\sigma}]_{j2} f\left(E_{\mathbf{k}}; \beta, \mu\right)
\end{aligned} \tag{A.15}$$

In the second passage this distribution appeared because an expectation value over a gas of free Φ fermions was taken. Such an expectation value admits no off-diagonal values, hence the $\delta_{i'j'}$. The diagonal entries are precisely the definition of the Fermi-Dirac distribution for the given energy. At zero temperature and half-filling, the lower band $-E_{\mathbf{k}}$ is completely filled while the upper band $E_{\mathbf{k}}$ is empty. Substituting $f = 1$ in the first term of line (A.15), $f = 0$ in the second and summing Δ_{12} and Δ_{21} as done in Eq. (A.13), it's easy to derive the result of Eq. (A.14). At finite temperature, following the lead of the above paragraph, the antiferromagnetic instability order parameter m will be given simply by

$$m = \frac{1}{2L_x L_y} \sum_{\mathbf{k}\in \mathrm{BZ}} \sum_{\ell=1}^{2} [W_{\mathbf{k}\uparrow}]_{\ell 1} [W^\dagger_{\mathbf{k}\uparrow}]_{2\ell} f\left((-1)^\ell E_{\mathbf{k}}; \beta, \mu\right) \tag{A.16}$$

Then: mean-field approximations yield an estimate for the magnetization at a given temperature and chemical potential just by carefully combining the elements of the diagonalizing matrix W of each Bogoliubov matrix $h_{\mathbf{k}\sigma}$.

A.3.5 The half-filled case

Consider specifically the half-filled situation. Since due to symmetry $\mu = 0$, we have the finite-temperature self-consistent equation

$$\begin{aligned}
m &= \frac{1}{L_x L_y} \sum_{\mathbf{k}\in \mathrm{MBZ}} \sin(2\theta_{\mathbf{k}}) \left[f\left(-E_{\mathbf{k}}; \beta, 0\right) - f\left(E_{\mathbf{k}}; \beta, 0\right)\right] \\
&= \frac{1}{2L_x L_y} \sum_{\mathbf{k}\in \mathrm{MBZ}} \frac{\Delta}{\sqrt{\epsilon^2_{\mathbf{k}} + \Delta^2}} \tanh\left(\frac{\beta}{2}\sqrt{\epsilon^2_{\mathbf{k}} + \Delta^2}\right)
\end{aligned}$$

Recalling that $m = \Delta/U$, the above equation becomes in thermodynamic limit $L \to \infty$

$$\frac{1}{U} \simeq \frac{1}{2} \int_{\mathrm{MBZ}} \frac{\mathrm{d}\mathbf{k}}{(2\pi)^2} \frac{1}{\sqrt{\epsilon^2_{\mathbf{k}} + \Delta^2}} \tanh\left(\frac{\beta}{2}\sqrt{\epsilon^2_{\mathbf{k}} + \Delta^2}\right)$$

Substitute the momentum integral with an integral over energies, in the low temperature limit, $\beta \to \infty$ (thus approximate the hyperbolic tangent with 1)

$$\frac{1}{U} \simeq \frac{1}{2} \int_{\mathrm{bands}} \frac{\mathrm{d}\epsilon \rho(\epsilon)}{\sqrt{\epsilon^2 + \Delta^2}}$$

[To be continued...]

A.3.6 Instability of the commensurate AF solution and atypical metallic bands

A key point to be discussed is the known instability of the AF HF solution of the EHM. As is thoroughly discussed in [9], the solution we presented above is only stable at half-filling, becoming

hardly unstable at infinitesimal doping. This is due to the commensurate nature of the established AF phase: we impose SSB to take place at wavevector $\boldsymbol{\pi}$, shrinking the BZ to exactly half its size and giving back on the newly defined MBZ two bands $\pm E_{\mathbf{k}}$. This procedure actually works well for the half-filled case: the magnetization essentially depends on the scattering rate between points on the FS connected by a $\boldsymbol{\pi}$ vector. The half filled case, taking advantage of the natural nesting property of the bare bands,

$$\forall \mathbf{k} \in \partial\text{MBZ} : \ \epsilon_{\mathbf{k}} = \epsilon_{\mathbf{k}+\boldsymbol{\pi}}$$

(being ∂MBZ the boundary of the MBZ) exhibits a magnetization at infinitesimal interaction. For a many body state resulting from continuous SSB, to establish a given phase means to show the presence of a stable gapless Goldstone mode associated to the broken symmetry. Such a Goldstone mode is essentially a sharp peak at zero frequency for some dressed response function. For the AF phase, it follows from the reduced $\mathrm{U}^z(1)$ rotational symmetry and is related to the proper transverse pseudospin-pseudospin response function, 2×2 matrix equation,

$$\tilde{\chi}_{\hat{\mathbf{S}}^-\hat{\mathbf{S}}^+}(\mathbf{k},\omega) = \frac{\chi_{\hat{\mathbf{S}}^-\hat{\mathbf{S}}^+}(\mathbf{k},\omega)}{1 - U\chi_{\hat{\mathbf{S}}^-\hat{\mathbf{S}}^+}(\mathbf{k},\omega)} \tag{A.17}$$

being χ the free transverse response. The pseudospin hereby considered is the one of Eq. (A.6). As is shown in [9], for the commensurate AF SSB at wavevector $\boldsymbol{\pi}$ the condition for the presence of a stable gapless mode reduces to a 2×2 matrix equation,

$$\text{Stability condition:} \qquad \mathbb{I}_{2\times 2} - U\left[\chi_{\hat{\mathbf{S}}^-\hat{\mathbf{S}}^+}(\boldsymbol{\pi},0)\right] \geq 0 \tag{A.18}$$

with $\left[\chi_{\hat{\mathbf{S}}^-\hat{\mathbf{S}}^+}(\boldsymbol{\pi},\omega)\right]$ the response function matrix obtained by considering a matrix response function for a two-sites unit cell. The above equation is to be interpreted as a matricial equation [Explain better..]. Considering the eigenvalue of largest amplitude of the matrix λ_δ at filling δ, the one most prone to instabilities, it is found that

$$\begin{aligned} \lambda_0(\mathbf{k} \to \boldsymbol{\pi}, 0) &= \frac{1}{U} && \text{(half filling)} \\ \lambda_\delta(\mathbf{k} \to \boldsymbol{\pi}, 0) &= \frac{1}{U} + \frac{2\epsilon_{\mathrm{F}}}{\Delta} N(\epsilon_{\mathrm{F}}) && \text{(finite doping)} \end{aligned}$$

The reason for the distinction above is the intrinsic metallic nature of the system for infinitesimal doping. At half-filling the system is an insulator, therefore no Fermi energy is defined, as well as no FS. Evidently this implies

$$\begin{aligned} &1 - U\lambda_0(\mathbf{k} \to \boldsymbol{\pi}, 0) = 0 \quad \text{(half filling)} && \implies \quad \text{stable Goldstone mode} \\ &1 - U\lambda_\delta(\mathbf{k} \to \boldsymbol{\pi}, 0) < 0 \quad \text{(finite doping)} && \implies \quad \text{unstable Goldstone mode} \end{aligned}$$

For any finite doping, the commensurate AF phase becomes unstable and is destroyed by transverse spin fluctuations. Nevertheless, for the sake of completeness and because we noticed too late, we will study the metallic AF also at finite doping.

A.3.7 Hartree-Fock algorithm results in reciprocal space

The above sections offer a self-consistency equation for the magnetization m; W is determined by m indeed. Then a self-consistent algorithm to search for a self consistent estimate for m may be sketched, following the general idea of Sec. **??**:

0. Algorithm setup: initialize a counter $i = 1$ and choose:

   - the local repulsion U/t or equivalently the hopping amplitude t/U;
   - the coarse-graining of the BZ, which is, fix L_x and L_y. Then

     $$k_x = 2\pi n_x / L_x \qquad k_y = 2\pi n_y / L_y$$

     where $-L_j/2 \leq n_j \leq L_j/2$, $n_j \in \mathbb{Z}$;

- the density n or equivalently the doping $\delta \equiv n - 0.5$;
- the inverse temperature β;
- the number of iterations $p \in \mathbb{N}$;
- the mixing parameter $g \in [0, 1]$;
- the tolerance parameters $\Delta_m, \Delta_n \in \mathbb{R}$ (respectively for magnetization and density);

1. Select a random starting value $m_0 \in [0, 1]$;
2. For each slot of the BZ, initialize the appropriate 2×2 matrix $h_{\mathbf{k}\uparrow}$ as in Eq. (A.5);
3. For the given hamiltonian, find the optimal chemical potential μ as follows:
   a) Diagonalize $h_{\mathbf{k}\uparrow}[m_0, U]$ and obtain its eigenvalues $\pm E_{\mathbf{k}}[m_0, U]$;
   b) Define the function of the chemical potential μ,
   $$\delta n(\mu; \beta, m_0, U) \equiv 2 \left[f\left(-E_{\mathbf{k}}[U, m_0]; \beta, \mu\right) + f\left(E_{\mathbf{k}}[U, m_0]; \beta, \mu\right)\right] - n$$
   c) Find the root of δn,
   $$\delta n(\mu_0) = 0$$
   Then μ_0 is the chemical potential which, at magnetization m_0, realizes the best approximation of density n;
4. Diagonalize the matrix $h_{\mathbf{k}\uparrow}$ and obtain $d_{\mathbf{k}\uparrow}$;
5. Compute m using Eq. (A.16) with chemical potential μ_0 and update the counter, $i \to i + 1$;
6. Check if $|m - m_0| \leq \delta_m$:
   - If yes, halt;
   - If not: check if $i > p$
     - If yes, halt and consider choosing better tolerance and model parameters;
     - If not, define
     $$m_0 = gm + (1 - g)m_0$$
     (logical assignment notation used) and repeat from step 2.

The algorithm sketched hereby was ran with the following setup:

```
UU = [U for U in 0.5:0.5:20.0]        # Local repulsions
LL = [256]                            # Lattice sizes
dd = [d for d in 0.0:0.05:0.45]       # Dopings
bb = [100.0, Inf]                     # Inverse temperatures
p = 100                               # Max number of iterations
dm = 1e-4                             # Tolerance on magnetization
dn = 1e-2                             # Tolerance on density
g = 0.5                               # Mixing parameter
```

In Fig. A.6 plots at $\beta = 100$ of the magnetization m is reported. As is evident in Fig. A.6a, doping disrupts AF ordering; the horizontal asymptote lowers as δ gets bigger, a mere consequence of the fact that the free space at each single-particle state in k-space shrinks as density increases; also, for $\delta > 0$, a finite magnetization m exists only for $U \geq U_c[\delta]$ (a critical value parametrically dependent on doping). Fig. A.6b shows the dependence of magnetization on doping at various fixed local repulsions U: once again, to dope the material disrupt AF ordering. Identical analysis have been performed for different temperatures, leading to analogous results as long as $\beta \gtrsim 10$ and to $m \simeq 0$ for higher temperatures (predictably).

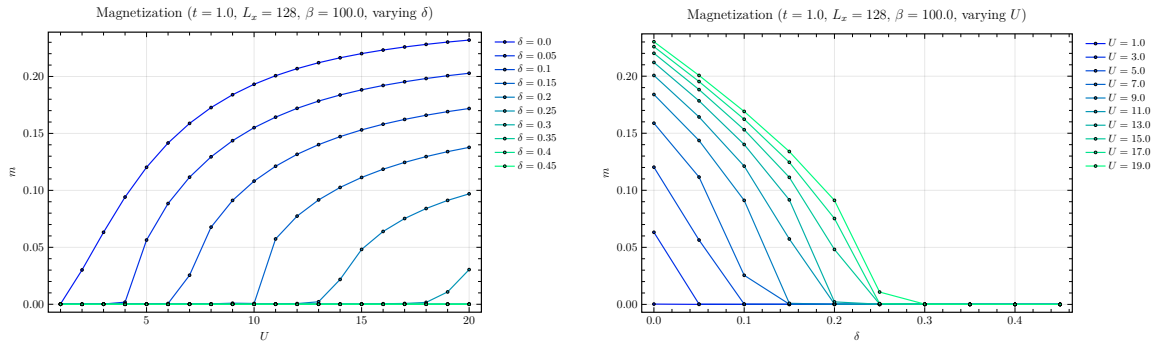

a | Local repulsion U/t depencence. b | Doping $\delta = n - 0.5$ dependence.

Figure A.6 | Plots of the zero-temperature AF instability order parameter m as a function of both the local repulsion U/t (Fig. A.6a) and the doping $\delta = n - 1/2$ (Fig. A.6b).

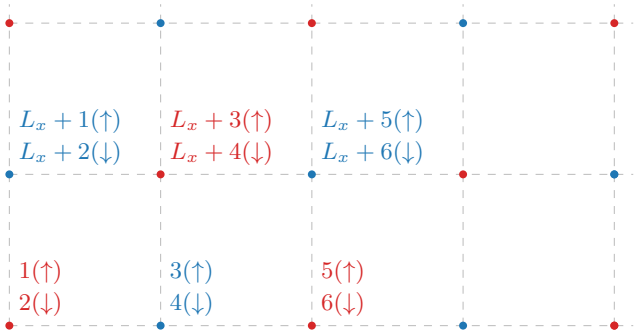

Figure A.7 | Schematics of the site ordering on a square lattice performed by sweeping along rows. Left-bottom side is one corner of the lattice. Red sites are characterized by $x + y$ being odd, blue sites by being even. The number reported near to each site is the α entry in the matrix representation for a finite square lattice.

A.3.8 An alternative (less efficient) real-space approach

The theoretical derivation of the above paragraphs offers a simple description of the system anti-ferromagnetic instability as the instauration of a ground-state of quasiparticles. Here a self-consistent algorithmic extraction of the expected magnetization is presented, following [8]. Note that this algorithm is by far the least efficient, being performed in real space with dimensional exponential scaling in terms of computational time. It is here presented just for completeness as an alternative derivation. This algorithm can become useful for simulations not preserving space-translational invariance, e.g. introducing some degree of disorder. Consider a square lattice of $L_x \times L_y$ sites: the hamiltonian will be a matrix of dimension $2L_xL_y \times 2L_xL_y$,

$$[\hat{H}]_{(\mathbf{r}\sigma)(\mathbf{r}'\sigma')} = \langle\Omega|\hat{c}_{\mathbf{r}\sigma}\hat{H}\hat{c}^{\dagger}_{\mathbf{r}'\sigma'}|\Omega\rangle$$

For simplicity, in the following $D \equiv 2L_xL_y$. In this context, the following convention is used: the rows/column index entry $\alpha = (\mathbf{r}\sigma)$ is associated to a specific site $\mathbf{r} = (x, y)$ and spin σ through the relation

$$\alpha = 2j_{\mathbf{r}} - \delta_{\sigma=\uparrow} \quad \text{where} \quad j_{\mathbf{r}} = x + (y-1)L_x$$

Let me break this through. For each site $\mathbf{r}$, two sequential indices are provided ($2j_{\mathbf{r}} - 1$, hosting spin $\uparrow$, and $2j_{\mathbf{r}}$, hosting spin $\downarrow$). $j_{\mathbf{r}}$ just orders the site rows-wise. This way, $(x, 1)$ is assigned to $j_{(x,1)} = x$, while its NN one site above $(x, 2)$ is assigned to an entry shifted by L_x, $j_{(x,2)} = x + L_x$. This is just a way of counting the site of a finite square lattice by sweeping along a row and then moving to the row above. Fig. A.7 reports a scheme of the used site ordering.

Within this convention, matrix elements $H_{\alpha\beta}$ are defined by:

- If $\sigma = \sigma'$ and $\mathbf{r}$, $\mathbf{r}'$ are NN, the matrix entry is $-t$. In terms of the used greek indices, α and β satisfy said requirement if $|\alpha - \beta| = 2$ (horizontal hopping) or $|\alpha - \beta| = 2L_x$ (vertical hopping). Along column α of the hamiltonian matrix, the elements $-t$ appear at positions

$$(\alpha \pm 2L_x) \mod D \quad \text{and} \quad (\alpha \pm 2) \mod D$$

- If $\mathbf{r} = \mathbf{r}'$ and $\sigma = \sigma'$ (along the diagonal), the local interaction with the mean field is given by the matrix element

$$-mU \times (-1)^{x+y} \times (-1)^{\delta_{\sigma=\downarrow}}$$

Starting from a given entry α, $j_{\mathbf{r}}$ is retrieved simply by $j_{\mathbf{r}} = \lfloor \alpha/2 \rfloor$, and then

$$x + y = (j_{\mathbf{r}} + 1) - \left\lfloor \frac{j_{\mathbf{r}}}{L_x} \right\rfloor (L_x - 1)$$

Then the $j_{\mathbf{r}}$-th 2×2 block along the diagonal will be given by

$$(-1)^{x+y} \underbrace{\begin{bmatrix} -mU & \\ & mU \end{bmatrix}}_{\mathcal{B}}$$

Note that the resulting block diagonal contribution to the hamiltonian is shaped like follows (assume L_x to be even):

$$\begin{array}{c} \\ 1 \\ 2 \\ \vdots \\ L_x - 1 \\ L_x \\ L_x + 1 \\ L_x + 2 \\ \vdots \end{array} \begin{array}{c} \begin{array}{cccccccc} 1 & 2 & \cdots & L_x - 1 & L_x & L_x + 1 & L_x + 2 & \cdots \end{array} \\ \begin{bmatrix} \mathcal{B} & & & & & & & \\ & -\mathcal{B} & & & & & & \\ & & \ddots & & & & & \\ & & & \mathcal{B} & & & & \\ & & & & -\mathcal{B} & & & \\ & & & & & -\mathcal{B} & & \\ & & & & & & \mathcal{B} & \\ & & & & & & & \ddots \end{bmatrix} \end{array}$$

Along the same row, on the diagonal the 2×2 blocks $\mathcal{B}$ alternate signs; changing row (in the example above, at positions $L_x, L_x + 1$), due to the anti-ferromagnetic configuration of local mean-fields, an additional -1 is included. If L_x is taken to be odd, the diagonal blocks just alternate signs all the way.

These prescriptions allow to build from scratch the hamiltonian matrix. After that, diagonalization provides D orthonormal eigenvectors $\mathbf{v}^\ell \in \mathbb{C}^{D \times D}$ with $\ell = 1, \cdots, D$, each associated to a precise eigenvalue $\epsilon^\ell \in \mathbb{R}$. At equilibrium, electrons will fill up the energy eigenstates according to,

$$\langle \hat{n}_{\mathbf{r}\sigma} \rangle = \sum_{\ell=1}^{D} \left| v_\alpha^\ell \right|^2 f(\epsilon^\ell; \beta, \mu) \quad \text{where} \quad \alpha = (\mathbf{r}\sigma)$$

For a fixed filling $n = N/D$, the chemical potential must satisfy

$$\begin{aligned} n &= \frac{1}{D} \sum_{\mathbf{r}\sigma} \langle \hat{n}_{\mathbf{r}\sigma} \rangle \\ &= \frac{1}{D} \sum_{\mathbf{r}\sigma} \sum_{\ell=1}^{D} \left| v_\alpha^\ell \right|^2 f(\epsilon^\ell; \beta, \mu) \\ &= \frac{1}{D} \sum_{\ell=1}^{D} f(\epsilon^\ell; \beta, \mu) \end{aligned}$$

since the $\mathbf{v}^\ell$ eigenvectors are orthonormal. The chemical potential for the half-filled model is already known to be

$$\mu\big|_{n=1/2} = -\frac{U}{2}$$

as evident from Eq. (A.3). Average magnetization is then given by

$$\begin{aligned} m &= \frac{1}{D}\sum_{\mathbf{r}}(-1)^{x+y}\left[\langle\hat{n}_{\mathbf{r}\uparrow}\rangle - \langle\hat{n}_{\mathbf{r}\downarrow}\rangle\right] \\ &= \frac{1}{D}\sum_{\lambda=1}^{D/2}(-1)^{(\lambda+1)-\lfloor\lambda/L_x\rfloor(L_x-1)}\sum_{\ell=1}^{D}\left[\left|v^\ell_{2\lambda-1}\right|^2 - \left|v^\ell_{2\lambda}\right|^2\right] f(\epsilon^\ell;\beta,\mu) \end{aligned} \tag{A.19}$$

since $\mathbf{r}\uparrow$ is associated to an odd index entry, while $\mathbf{r}\downarrow$ to the following even entry. The associated HF algorithm is identical to the one presented in Sec. A.3.7, with the following substitutions:

2. Initialize the hamiltonian matrix $H_{\alpha\beta}$ matrix according to the initialized m_0 and the site indexing rules of Fig. A.7;

4. Diagonalize the matrix associated to the operator $\hat{H}_{\alpha\beta} - \mu\hat{N}$ collecting the $\mathbf{v}^\ell$ eigenvectors;

5. Compute m using Eq. (A.19) and update the counter, $i \to i+1$;

A.4 (Impossibility of) BCS-like superconducting phase

[To be continued...]

Bibliography

[1] Daniel P. Arovas et al. "The Hubbard Model". In: *Annual Review of Condensed Matter Physics* 13.Volume 13, 2022 (2022), pp. 239–274. ISSN: 1947-5462. DOI: https://doi.org/10.1146/annurev-conmatphys-031620-102024. URL: https://www.annualreviews.org/content/journals/10.1146/annurev-conmatphys-031620-102024.

[2] Zhangkai Cao et al. "Dominant p-wave pairing induced by nearest-neighbor attraction in the square-lattice extended Hubbard model". In: *Phys. Rev. B* 111 (2 Jan. 2025), p. 024509. DOI: 10.1103/PhysRevB.111.024509. URL: https://link.aps.org/doi/10.1103/PhysRevB.111.024509.

[3] Piers Coleman. *Introduction to Many-Body Physics*. Cambridge University Press, 2015.

[4] Michele Fabrizio. *A Course in Quantum Many-Body Theory*. Springer, 2022.

[5] Gabriele Giuliani and Giovanni Vignale. *Quantum Theory of the Electron Liquid*. Cambridge University Press, 2005.

[6] Giuseppe Grosso and Giuseppe Pastori Parravicini. *Solid State Physics*. Second Edition. Academic Press, 2014.

[7] J. E. Hirsch. "Two-dimensional Hubbard model: Numerical simulation study". In: *Phys. Rev. B* 31 (7 Apr. 1985), pp. 4403–4419. DOI: 10.1103/PhysRevB.31.4403. URL: https://link.aps.org/doi/10.1103/PhysRevB.31.4403.

[8] Robin Scholle et al. "Comprehensive mean-field analysis of magnetic and charge orders in the two-dimensional Hubbard model". In: *Phys. Rev. B* 108 (3 July 2023), p. 035139. DOI: 10.1103/PhysRevB.108.035139. URL: https://link.aps.org/doi/10.1103/PhysRevB.108.035139.

[9] Avinash Singh and Zlatko Tešanović. "Collective excitations in a doped antiferromagnet". en. In: *Physical Review B* 41.1 (Jan. 1990), pp. 614–631. ISSN: 0163-1829, 1095-3795. DOI: 10.1103/PhysRevB.41.614. URL: https://link.aps.org/doi/10.1103/PhysRevB.41.614 (visited on 12/12/2025).

[10] Alexander Wietek et al. "Stripes, Antiferromagnetism, and the Pseudogap in the Doped Hubbard Model at Finite Temperature". en. In: *Physical Review X* 11.3 (July 2021), p. 031007. ISSN: 2160-3308. DOI: 10.1103/PhysRevX.11.031007. URL: https://link.aps.org/doi/10.1103/PhysRevX.11.031007 (visited on 12/12/2025).